Hydrol. Earth Syst. Sci., 30, 317–341, 2026
https://doi.org/10.5194/hess-30-317-2026

Hydrology and Earth System Sciences
Open Access
EGU

Insights into evapotranspiration partitioning based on hydrological observations using the generalized proportionality hypothesis

Amin Hassan[1], **Iain Colin Prentice**[2,3], **and Xu Liang**[1]

[1]Department of Civil and Environmental Engineering, University of Pittsburgh, Pittsburgh, Pennsylvania, 15213, USA
[2]Georgina Mace Centre for the Living Planet, Department of Life Sciences, Imperial College London, Silwood Park Campus, Ascot, UK
[3]Department of Earth System Science, Ministry of Education Key Laboratory for Earth System Modeling, Institute for Global Change Studies, Tsinghua University, Beijing, China

Correspondence: Xu Liang (xuliang@pitt.edu)

Received: 10 February 2025 – Discussion started: 11 March 2025
Revised: 18 October 2025 – Accepted: 28 November 2025 – Published: 23 January 2026

Abstract. Evapotranspiration comprises transpiration, soil evaporation, and interception. The partitioning of evapotranspiration is challenging due to the lack of direct measurements and uncertainty of existing evapotranspiration partitioning methods. We propose a novel method to estimate long-term mean transpiration to evapotranspiration (E_t/E) ratios based on the generalized proportionality hypothesis using long-term mean hydrological observations at the watershed scale. We tested the method using 648 watersheds in the United States classified into six vegetation types. We mitigated impacts of the variability associated with different E_p data products by rescaling their original E_p values using the product E/E_p ratios in combination with the observed E calculated from watershed water balance. With E_p thus rescaled, our method produced consistent E_t/E across six widely used E_p products. Shrubs (0.33) and grasslands (0.32) showed lower mean E_t/E than croplands (0.48) and forests (respectively 0.69, 0.60, and 0.70 for evergreen needleleaf, deciduous broadleaf, and mixed forests). E_t/E showed significant dependence on aridity, leaf area index, and other hydrological and environmental conditions. Using E_t/E estimates, we calculated transpiration to precipitation ratios (E_t/P) ratios and revealed a bell-shaped curve at the watershed scale, which conformed to the bell-shaped relationship with the aridity index (AI) observed at the field and remote-sensing scales (Good et al., 2017). This relationship peaked at an E_t/P between 0.5 and 0.6, corresponding to an AI between 2 and 3 depending on the E_p dataset used. These results strengthen our understanding of the interactions between plants and water and provide a new perspective on a long-standing challenge for hydrology and ecosystem science.

1 Introduction

Partitioning evapotranspiration is important for understanding water and energy balances of terrestrial ecosystems. Evapotranspiration has been predicted to increase at the expense of soil moisture due to climate change (Li et al., 2022; Niu et al., 2019) with potential implications for future projections of water, energy, and carbon balances. Large uncertainty remains in the partitioning of evapotranspiration into its components: transpiration, interception, and bare soil evaporation. Various methods have been developed to partition evapotranspiration based on measurements (Kool et al., 2014; Stoy et al., 2019). These include (1) flux-variance similarity methods using high frequency (10–20 Hz) flux tower measurements, which estimate E_t/E based on carbon-water correlation since transpiration and plant carbon uptake are concurrent (Scanlon and Kustas, 2010, 2012; Scanlon and Sahu, 2008; Skaggs et al., 2018); (2) eddy-covariance methods, which estimate E_t/E using assumptions related to water use efficiency based on widely available half-hourly/hourly eddy covariance measurements (Berkelhammer et al., 2016; Li et al., 2019; Scott and Biederman, 2017; Yu et al., 2022; Zhou et al., 2016); and (3) isotopic methods (Griffis, 2013; Williams et al., 2004; Zhang et al., 2011). Measurements of

sap flow through plant stems have also been commonly used to more directly estimate transpiration. Sap flow measurements are classified into three groups (Kool et al., 2014): heat balance methods (Čermák et al., 1973; Sakuratani, 1981, 1987), heat pulse methods (Cohen et al., 1981; Green et al., 2003; Swanson and Whitfield, 1981), and constant heater methods (Čermák et al., 2004; Granier, 1985). Poyatos et al. (2021) compiled 202 sap flow datasets to form the global SAPFLUXNET dataset. Recent studies have used remotely sensed solar-induced fluorescence (SIF) measurements (Alemohammad et al., 2017; Damm et al., 2018; Liu et al., 2022; Lu et al., 2018; Pagán et al., 2019; Shan et al., 2019) to estimate global transpiration, relying on the close coupling between transpiration and photosynthesis.

The ratio of transpiration to evapotranspiration (E_t/E) is a particularly important quantity because the controls on T (which is tightly regulated by plants through stomatal behavior) are substantially different from the controls on the other two components. The evapotranspiration partitioning methods summarized above have multiple limitations and produce an alarmingly wide range of values for the global mean E_t/E. Wei et al. (2017) showed mean global E_t/E varying from 0.24 to 0.90 based on a variety of remote-sensing, isotopic, and modelling studies. Another compilation by Liu et al. (2022) showed the mean varying between 0.24 and 0.86. Schlesinger and Jasechko (2014) showed that E_t/E ratios derived from isotopic methods tend to be systematically higher than those produced by other methods. It has also been shown that two different evapotranspiration partitioning methods could produce greatly different E_t/E values at the same site (Cavanaugh et al., 2011; Moran et al., 2009). Some E_t/E estimates at the stand scale ignore transpiration from subcanopy vegetation, resulting in underestimation (Schlesinger and Jasechko, 2014). There is no consensus on which method is more accurate (Stoy et al., 2019); this presents a challenge for applying the E_t/E estimates using any of the above methods, especially when they are developed based on data at site scale but are applied at larger (regional to global) spatial scales.

Few studies have considered partitioning evapotranspiration based on hydrological concepts using widely available long-term hydrological observations, which could in principle provide reliable methods to estimate E_t/E. Gerrits et al. (2009) estimated monthly and (upscaled) annual transpiration based on precipitation, interception, soil moisture, and the aridity index. They estimated E_t/E by modeling interception (which includes topsoil evaporation) as a daily threshold process (threshold is the interception storage capacity) and used rainfall distributions to upscale it to the monthly and then annual interception. Transpiration was modeled as a monthly threshold process based on net rainfall (precipitation minus interception), with the threshold being the soil moisture storage estimated based on a hydrological model, and upscaled it to annual transpiration via a rainfall distribution. E_t/E is then calculated by assuming evapotranspiration is interception plus transpiration, since topsoil evaporation is included in interception, and deeper soil and open water evaporations are neglected. Mianabadi et al. (2019) extended their approach and applied it globally. In this study, we propose a new method to partition evapotranspiration based on the Generalized Proportionality Hypothesis (GPH) using long-term hydrological observations. The GPH was initially used by the United States Soil Conservation Service (SCS) for runoff calculation (USDA SCS, 1985) and was afterwards generalized by Ponce and Shetty (1995a, b). Wang and Tang (2014) provided a comprehensive discussion of the use of GPH and noted its connection to various models, including the "abcd" model, the SCS direct runoff model, and the Budyko-type models. The GPH partitions water fluxes into their components and has been implemented as a two-stage partitioning. The first stage partitions precipitation into soil wetting and surface runoff; the second stage partitions soil wetting into baseflow and evaporation (Ponce and Shetty, 1995a, b; Tang and Wang, 2017). We follow an approach based on the GPH partitioning of soil wetting to estimate catchment E_t/E based on hydrological observations. Due to the wider availability of hydrological observations compared to the observations required for the techniques previously mentioned, this method has a wide potential for application in gauged watersheds across the globe.

The objectives of our study are: (1) to develop a new method to estimate E_t/E at the catchment scale based on long-term hydrological observations, (2) to test the method and evaluate its robustness to different data products using watersheds with different vegetation types, (3) to find E_t/P (transpiration/precipitation) ratios based on E_t/E and to compare this to previous studies, and (4) to understand the effect of hydrological and environmental conditions on both E_t/E and E_t/P. The paper is organized as follows. Section 2 describes the newly developed method and the datasets used. Section 3 investigates the differences in potential evapotranspiration (E_p) data products, and the use of a rescaled E_p for E_t/E estimation. Section 4 presents the results from the new method. Section 5 discusses the results and investigates their dependence on hydrological and environmental factors. Section 6 provides an insight into the variation of some existing partitioning methods. Section 7 summarizes our conclusions.

2 Methods and data

2.1 Theory

We present a new method to estimate long-term mean E_t/E ratios at a watershed scale by taking advantage of long-term available hydrological observations. The new method is based on the Generalized Proportionality Hypothesis (GPH), shown in Eq. (1). The GPH equation has been previously established in the literature based on the observed relationships found by L'Vovich (1979) and the later mathematical

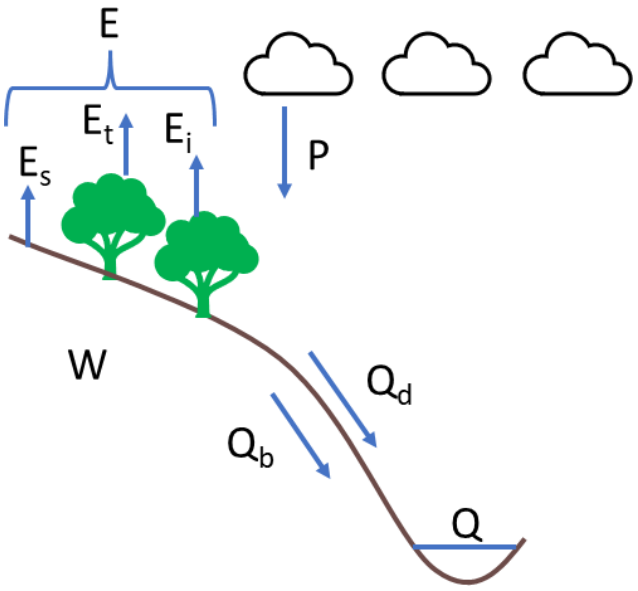

Figure 1. Two stage partitioning of annual precipitation. E: evapotranspiration; E_s: soil evaporation; E_i: interception evaporation; E_t: transpiration; P: precipitation; W: soil wetting; Q_b: baseflow; Q_d: direct runoff; Q: total runoff.

derivation (and generalization) by Ponce and Shetty (1995a, b). The proportionality hypothesis of the SCS method was obtained based on observed data from a larger number of watersheds (USDA SCS, 1985), which was then generalized by Ponce and Shetty (1995a). GPH partitions an unbounded water quantity Z into an unbounded water quantity Y and a water quantity X that is bound by its potential value X_p. The value X_0 is the initial quantity of X that is fulfilled prior to the competition between X and Y; for example, interception is a portion of E that is initially lost and not accessible for baseflow:

$$\frac{X - X_0}{X_p - X_0} = \frac{Y}{Z - X_0} \tag{1}$$

Ponce and Shetty (1995a, b) applied the GPH for hydrological partitioning. They partitioned annual precipitation over two stages: the first stage partitions precipitation into catchment wetting and surface runoff; and the second stage partitions wetting (W) into evapotranspiration (E) and baseflow (Q_b) as shown in Fig. 1. Both stages of partitioning follow the generalized formula in Eq. (1). The two-stage partitioning is well established, has been proved with thermodynamic principles (Wang et al., 2015), and has been extensively used in the literature in studies (Abeshu and Li, 2021; Chen and Wang, 2015; Sivapalan et al., 2011; Tang and Wang, 2017; Wang and Tang, 2014).

In this work, we use the second stage partitioning to partition wetting into evapotranspiration and baseflow as shown in Eq. (2):

$$\frac{E - E_0}{E_p - E_0} = \frac{Q_b}{W - E_0} \tag{2}$$

where E_0 is the initial evapotranspiration that does not compete with baseflow and E_p is the potential evapotranspiration. W can be estimated from watershed balance as $P - Q_d$, where P is precipitation and Q_d is direct runoff. E can be estimated from watershed balance as $P - Q$, where Q is the total runoff (since the long-term mean soil moisture change can be ignored). Initial evapotranspiration (E_0) has been represented in different ways in the literature. Ponce and Shetty (1995a, b) and Sivapalan et al. (2011) used λE_p to represent E_0, where λ is a coefficient, Tang and Wang (2017) and Wang and Tang (2014) used λW, and Abeshu and Li (2021) used λE. In this study, we choose λE as E_0 due to the interpretability of the λ parameter. We alternately use k instead of λ to avoid confusion with the latent heat of vaporization, leading to Eq. (3):

$$\frac{E - kE}{E_p - kE} = \frac{Q_b}{W - kE} \tag{3}$$

In Abeshu and Li (2021), E_0 included interception, evaporation from surface depression, topsoil evaporation, and shallow transpiration. In Gerrits et al. (2009), they assumed that interception includes canopy and understory interception, in addition to topsoil evaporation, while deep soil evaporation is insignificant or can be combined with interception. In Savenije (2004), they considered topsoil evaporation to be a part of interception, and distinguished transpiration between fast and slow ones, where fast transpiration relies on moisture in the top 50 cm of soil, and slow transpiration relies on deeper soil moisture. Therefore, we assume that E_0 includes bare soil evaporation, interception, and a portion (f) of the transpiration (E_t) representing the fast transpiration from the top 10 cm of soil (Abeshu and Li, 2021; Savenije, 2004). Since root uptake not only occurs near the surface but also progresses downwards (Gardner, 1983), we assume that transpiration extracted from the topsoil occurs in a rapid manner that makes it inaccessible to the competition between baseflow and E, and therefore belongs to E_0. Therefore, E_0 includes all evaporative fluxes except slow transpiration, meaning that slow transpiration is the only evaporative flux that competes with baseflow. Slow transpiration can therefore be expressed as $E_{t\_slow} = E - E_0$. For transpiration, we define fast transpiration as $E_{t\_fast} = f\,E_t$, and thus slow transpiration as $E_{t\_slow} = (1-f)\,E_t$. Equating these two E_{t_slow} equations yields $E - E_0 = (1-f)\,E_t$. Substituting E_0 with kE yields $(1-k)\,E = (1-f)\,E_t$, and thus we can get:

$$\frac{E_t}{E} = \frac{1-k}{1-f} \tag{4}$$

Equation (4) indicates that E_t/E can be found using k and f values. The k parameter can be found by applying an

optimization technique that maximizes the non-parametric Kling-Gupta efficiency (KGE, Eq. 5, Gupta et al., 2009; Pool et al., 2018) between observed soil wetting (from watershed balance, Eq. 6) and simulated soil wetting (rearranging Eq. 3 to be in terms of soil wetting, Eq. 7).

$$\mathrm{KGE} = 1 - \sqrt{(r-1)^2 + (\alpha-1)^2 + (\beta-1)^2} \tag{5}$$

where r is Pearson correlation coefficient, α is relative variability in the simulated and observed values, and β is the ratio between the mean simulated and mean observed flows.

From the water balance equation at the watershed scale, we obtain observed wetting as:

$$W_{\mathrm{obs}} = P - Q_{\mathrm{d}} \tag{6}$$

And by rearranging Eq. (3) to obtain simulated wetting:

$$W_{\mathrm{sim}} = Q_{\mathrm{b}} \frac{E_{\mathrm{p}} - kE}{E - kE} + kE \tag{7}$$

Since f represents the fast response of transpiration, we follow a similar approach to Abolafia-Rosenzweig et al. (2020) in defining the ratio of surface transpiration using root distribution and soil water stress. We additionally distinguish between energy- and water-limited regions by constraining energy-limited f using the aridity index as displayed in Eq. (8):

$$f = r_{10} \times S \times f_{\mathrm{AI}} \tag{8}$$

Where r_{10} is the root percentage in the top 10 cm of the soil, S is the soil moisture availability, and f_{AI} represents impact of available energy. If the aridity index ($\mathrm{AI} = E_{\mathrm{p}}/P$) is less than 1, the region is energy limited. Thus, $f_{\mathrm{AI}} = \mathrm{AI}$. If $\mathrm{AI} \geq 1$, then $f_{\mathrm{AI}} = 1$. The rationale behind this is that when $\mathrm{AI} < 1$, only a fraction of the transpiration from the top surface layer is quantified to be part of the fast components due to its energy limited nature.

The literature shows variation in how the depth of fast transpiration is defined. For example, Abolafia-Rosenzweig et al. (2020) used the top 5 cm to estimate transpiration from the surface soil layer. Wang et al. (2021) indicated that evapotranspiration occurs most rapidly from the top 10 cm of soil, with deeper layer responding more slowly. Similarly, Zhang et al. (2022) reported that rapid soil moisture responses to rainfall were concentrated in the top 5–10 cm, suggesting that fast transpiration is likely driven by increased soil moisture within this layer. By contrast, Abeshu and Li (2021) used 50 cm as the depth of the rapid response. We consider 50 cm to be an overestimation, as for some vegetation types (e.g., grasses) this depth may encompass nearly the entire rooting zone. Based on this evidence, we adopted 10 cm as the representative depth for fast transpiration. In addition, we conducted a sensitivity analysis in Sect. 4.4 to quantify the effect of this depth choice on the E_{t}/E values.

The soil moisture availability, S, represents the moisture availability in the root zone for root water uptake. Abolafia-Rosenzweig et al. (2020) calculated the soil moisture availability as a function of soil moisture, wilting point, and field capacity. To rely on hydrological observations instead of simulated or remotely sensed soil moisture, we assume the soil moisture availability to be represented by the ratio between baseflow and total streamflow (Q_{b}/Q). This ratio can give an indication of water availability in the soil and hence can be used to indicate soil moisture availability. Since we apply this method at the watershed scale, there may be multiple vegetation types in the same watershed, and therefore, we calculate a weighted value of f.

2.2 Data

From Eqs. (2)–(5) and the descriptions of Sect. 2.1, we see that one needs long-term observed precipitation, streamflow, baseflow, estimated E_{p}, and root distribution to estimate the E_{t}/E ratio. Watershed boundaries and precipitation data were retrieved from the Hydrometeorological Sandbox – École de technologie supérieure (HYSETS) dataset (Arsenault et al., 2020). The HYSETS dataset includes watershed boundaries, land cover, soil properties, meteorology, and hydrological data for 14 425 watersheds in North American. We selected 648 watersheds (Fig. 2) across the United States with at least 10 years of streamflow data between 1980 and 2018 from this HYSETS data source. Detailed land cover data were retrieved from the ESA CCI Land Cover project (https://www.esa-landcover-cci.org, last access: 28 December 2022).

Streamflow data were retrieved from the US Geological Survey (USGS), and their corresponding baseflow magnitudes were estimated by separating it from the streamflow data using a one-parameter digital filter separation method (Lyne and Hollick, 1979). Filtering methods separate direct runoff and baseflow by differentiating them based on frequency spectrums of the hydrograph, where low frequency flow represents baseflow and high frequency represents the direct runoff which has rapid responses to precipitation. We employed the widely used filtering method tool developed by Purdue University, Web-based Hydrological Analysis Tool (WHAT, Lim et al., 2005, 2010 , https://app.envsys.co.kr/what2020/index.php, last access: 18 December 2025), to separate baseflow from the observed streamflow. We set the value of the filter parameter to be 0.925 which is within the suggested range. We did a sensitivity analysis (in a separate study) and used different filter values and methods available from WHAT, the results were similar. Since other methods such as Eckhardt (2005) require knowledge of hydrogeological conditions, we chose the one-parameter digital filter method due to its simplicity and constant parameter value, which produces plausible results (Eckhardt, 2008; Xie et al., 2020). Additional details on the baseflow separation method are presented in Lim et al. (2005).

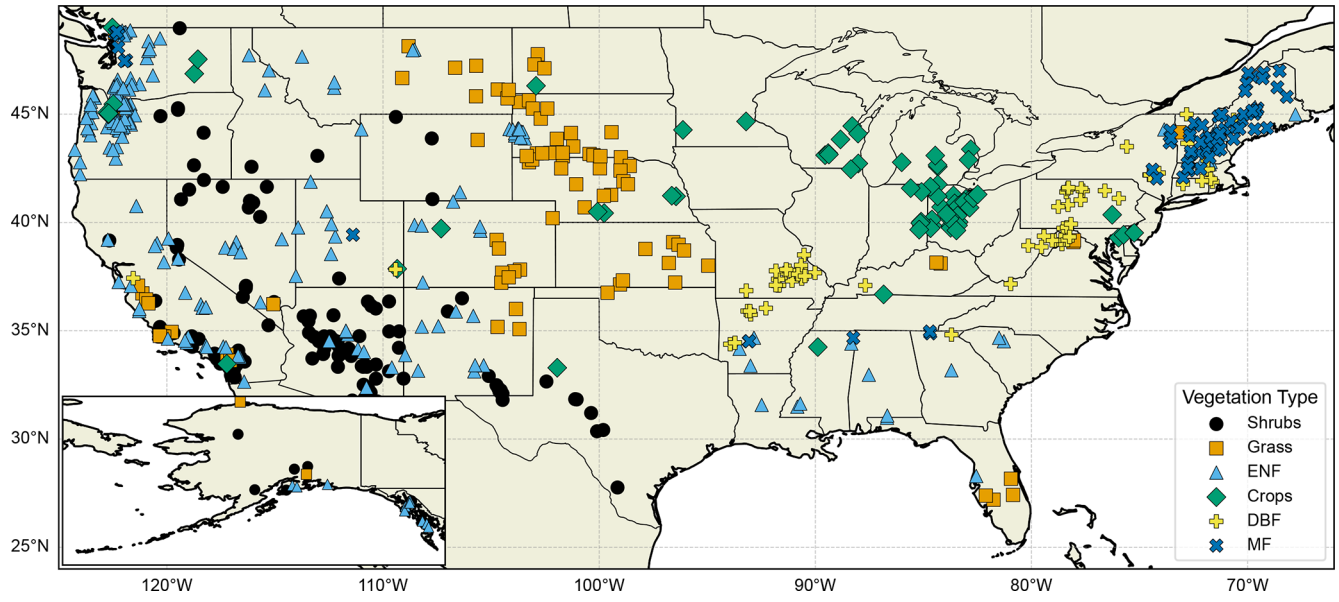

Figure 2. 648 watersheds in the US, categorized into six vegetation types; crops, grass, shrubs, evergreen needleleaf forest (ENF), deciduous broadleaf forests (DBF), and mixed forests (MF). The inset map at the bottom left shows watersheds in Alaska.

Information related to root density functions was obtained from Zeng (2001), who represented root density distribution as a two-parameter function for each vegetation type based on a compiled root database. The root density distribution from Zeng (2001) was validated using root information from other studies (Fan et al., 2016; Jackson et al., 1996; Lozanova et al., 2019; Schenk and Jackson, 2002; Wallace et al., 1980). Soil moisture stress (Q_b/Q) was calculated based on the USGS observed streamflow and the estimated baseflow from WHAT.

Numerous E_p data products are available that satisfy our study regions and time period requirements, posing a question as to which one should be selected – as each has its own strengths. To address this question, we examined six widely used E_p data products and assessed their impact on the estimation of E_t/E ratios. These data products were selected because they are (1) widely used within the hydrological and ecological communities, (2) associated with a wide range of spatial resolutions, and (3) derived using different methods. The six E_p datasets are the Global Land Evaporation Amsterdam Model (GLEAM v3.5a, Martens et al., 2017), the Moderate Resolution Imaging Spectroradiometer (MODIS MOD16A3GF) product (Running et al., 2022), the E_p dataset from Zhang et al. (2010), the North American Regional Reanalysis (NARR, Mesinger et al., 2006), the Simple Process-Led Algorithms for Simulating Habitats (SPLASH v2.0, Sandoval et al., 2024) , and the Breathing Earth System Simulator (BESS v2, Li et al., 2023). Details of these six products are provided in Table 1.

Environmental variables – relative humidity, downward shortwave radiation, air temperature, wind speed, and soil moisture content – were retrieved from the NARR dataset to study the dependencies of E_t/E on environmental factors. Data on leaf area index (LAI) were obtained from the Global Monthly Mean Leaf Area Index Climatology produced by ORNL DAAC (Mao and Yan, 2019) and aggregated to obtain the long-term mean LAI at watershed scale.

The relevant data were collected for 648 watersheds and aggregated to the annual timescale. The dominant vegetation type was determined for each watershed from the ESA CCI land cover data, and watersheds were classified into six vegetation types: crops, grass, shrubs, evergreen needleleaf forest (ENF), deciduous broadleaf forest (DBF), and mixed forest (MF). We assume each watershed has a single mean long-term E_t/E value. For each dataset, due to the different time coverage of the datasets and the streamflow gauges, we filtered the watersheds to include only those that have available data for at least 10 years. We used optimization to find k. We then performed additional filtering for each dataset to remove watersheds with KGE values less than zero. Using the filtered watersheds, we calculated E_t/E based on estimated k and f together with the other variables. The final number of watersheds associated with each dataset used in this study, after filtering, is shown in Table 2.

3 Impact of E_p products

Figure 3a shows mean annual E_p values from six different data products for the 648 study watersheds. We observe large differences in mean annual E_p among the six different data products. The differences in E_p are likely attributed to variations in input data and parameter values used by these prod-

Table 1. Description of six E_p products used in this study.

Dataset	E_p equation	Spatial and temporal scale	Remarks
GLEAM v3.5a	Priestley-Taylor	$0.25 \times 0.25°$, Daily/Monthly, 1980–2021	
NARR	Eta Model (Penman based)	32×32 km, Daily/Monthly, 1979–2022	
MODIS MOD16A3GF	Combination of Penman-Monteith and Priestley-Taylor	500×500 m, 8 d/Yearly, 2000–2021	
SPLASH v2	Priestley-Taylor	1 km, Daily, 1980–2018	Forced using daily DayMet (Thornton et al., 2022) data
BESS v2	Priestley-Taylor	5 km, Monthly, 1982–2022	
Zhang	Penman-Monteith	8×8 km, Daily/Monthly, 1983–2006	

Table 2. Number of filtered watersheds for each potential evapotranspiration (E_p) data product. Watersheds with less than 10 years of data and/or with Kling-Gupta efficiencies less than zero were removed from the analysis. Numbers are shown for each of the six vegetation types.

Type	All watersheds	NARR	MODIS	Zhang	GLEAM v3.5a	BESS v2	SPLASH v2
Crops	74	72	61	57	73	59	71
Grass	89	84	66	73	86	79	81
Shrubs	146	131	107	114	134	128	131
ENF	206	166	118	118	173	161	156
DBF	65	65	61	54	65	64	65
MF	68	63	58	52	66	51	61
Total	648	581	471	468	597	542	565

ucts, while differences in methods and resolutions used to compute E_p may play a secondary role (Hassan et al., 2024). Discrepancies between the input net radiation used in different data products result in especially large variations in the computed E_p. Variations in parameter values, including the Priestley-Taylor α parameter, among different data products also result in significant differences in the resulting E_p. On the other hand, the E/E_p ratios from the six different E_p products are relatively consistent among the six datasets (except for GLEAM) as shown in Fig. 3b. This is likely because within each product the same input/forcing data and parameter values are employed for both E_p and E, resulting in similar impacts on both. Such consistency is an indication of a uniformity of the underlying physics across these five products, despite the large disparities in their individual E_p magnitudes. The GLEAM E_p product, which has also been previously identified for its overestimation of E/E_p ratio by Peng et al. (2019) in comparison with FLUXNET E/E_p, appears to be an exception. Rather than excluding the GLEAM data product, we opted to adjust its E/E_p ratio by normalizing it with the average ratio of the other five datasets (NARR, MODIS, Zhang, SPLASH v2, and BESS v2), yielding an adjusting factor of 0.7. This adjusting factor of 0.7 was applied to GLEAM to adjust its E/E_p values. In addition, rescaled E_p values from the six data products in this study were newly derived by applying their individual E/E_p ratios, obtained from their own data products, to the watershed E values calculated based on watershed balance (i.e., $E = P - Q$) for each watershed. The importance of deriving E_p values for each data product through this rescaling approach (referred to as rescaled E_p), rather than using the original E_p product, is to ensure consistency between the E_p values and the watershed-budget estimated E values for each watershed while preserving the E/E_p ratios from the individual products. This is necessary because the magnitudes of some original E_p products are smaller than their corresponding watershed-budget estimated E values.

In essence, we derive new E_p values for all six products using Eq. (9), maintaining the E/E_p ratio for each data product (except for GLEAM, whose E/E_p ratio is adjusted by a factor of 0.7). This approach yields consistent E_p values across the 648 watersheds for each individual data product and captures the essential variations among the six E_p datasets. The rescaled E_p values obtained from Eq. (9) uphold the fundamental principles of individual products by preserving their respective E/E_p ratios. By doing so, the effects stemming

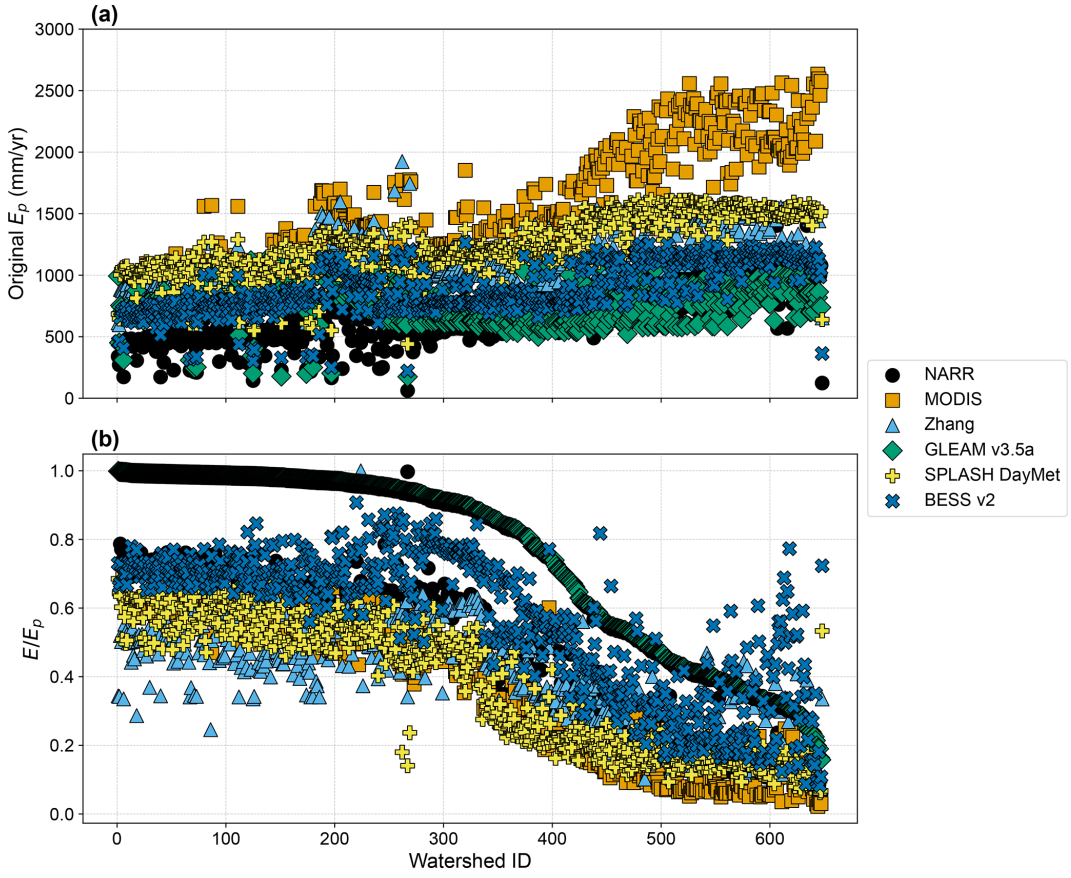

Figure 3. Original $E_\mathbf{p}$ for six data products: NARR, MODIS, Zhang, GLEAM v3.5a, SPLASH v2, and BESS v2 for 648 watersheds. (a) $E_\mathbf{p}$ values retrieved from the data products, and (b) E/$E_\mathbf{p}$ ratios retrieved from the data products. Watersheds are sorted in descending order according to GLEAM's E/$E_\mathbf{p}$.

from differences or uncertainties in their inputs/forcing data are notably mitigated, as the new E_p values are calculated using the watershed-budget estimated E and their own E/E_p ratios. This concept is akin to the notion of emergent constraints employed by others (Green et al., 2024; Hall et al., 2019; Williamson et al., 2021).

$$E_{p_\mathrm{rescaled}} = \frac{E_{p_\mathrm{dataset}}}{E_\mathrm{dataset}} \times E_\mathrm{obs} \tag{9}$$

where E_dataset and E_{p_dataset} are E and E_p values extracted from different data products, and E_obs is the watershed-budget estimated E calculated as $P - Q$ based on observed P and Q for each watershed. Table 3 shows the correlation between the rescaled E_p values of the six data products; the correlations show good consistency between the rescaled E_p values. These six rescaled E_p data products are then applied to Eqs. (2)–(5) to obtain E_t/E ratios for each of the six vegetation types over the 648 watersheds. With the six rescaled E_p data products, we can assess how variations in E_p affect the robustness of our new method in estimating E_t/E.

4 Results

4.1 *k* values

Figure 4 shows an example of the optimization between observed soil wetting (W_obs) and the simulated soil wetting (W_sim) with the optimized k value for a representative watershed of each vegetation type. Figure 5 shows the estimated values of k for the 648 watersheds using each of the six input datasets based on Eqs. (5)–(7). The six datasets show similar trends, where the highest k values are observed for the shrubs and grass vegetation types. Crops have lower k values than shrubs and grass, but equal or higher than those for forests according to the dataset used. Figure 5 illustrates that the greatest variations among the six data products occur in the mixed forest and crops. This discrepancy may be attributed to differences in how each data product defines mixed forest and crop compositions, resulting in varying estimated parameters. The k values observed in our study are similar in trend to those reported by Abeshu and Li (2021), but lower in magnitude. This difference is likely due to differences in input data to the GPH equation such as precipitation and PET values

Table 3. Correlations between rescaled E_p of six data products: NARR, MODIS, Zhang, GLEAM v3.5a, SPLASH v2, and BESS v2 for 648 watersheds.

	MODIS	GLEAM	NARR	SPLASH v2	BESS v2	Zhang
MODIS	1					
GLEAM v3.5a	0.72	1				
NARR	0.81	0.83	1			
SPLASH v2	0.80	0.84	0.83	1		
BESS v2	0.92	0.78	0.73	0.75	1	
Zhang	0.70	0.83	0.68	0.69	0.92	1

since different datasets are used for both studies. Sivapalan et al. (2011) reported lower k values (between 0 and 0.45). However, their definition of k differs from ours: while we define $E_0 = kE$ in Eq. (3), they adopted the formulation of $E_0 = kEp$. Since actual evapotranspiration (E) is typically much smaller than potential evapotranspiration (E_p), it is expected that their k values are lower than ours. In addition, the analysis of Sivapalan et al. (2011) was limited to 12 watersheds under relatively humid conditions (maximum aridity of 2.29), which does not capture the full range of climatic conditions, particularly drier environments.

4.2 f values

Figure 6 shows the values of the f parameter for 648 watersheds classified into six vegetation types. The highest f value is observed in grass, which can be explained by their shallow rooting depths causing higher portions of fast transpiration. The lowest f values are observed in forests due to their deeper rooting system, which provides access to deeper soil moisture, reducing the portion of fast transpiration.

4.3 E_t/E values

E_t/E ratios are shown in Fig. 7 and Table 4. Overall, the trend is consistent among the six datasets. Grass and shrubs have the lowest E_t/E values, with mean E_t/E in the range of 0.25–0.41. Crops have higher mean E_t/E ratios, with NARR, Zhang, and GLEAM averaging around 0.5, while MODIS shows a higher crop mean E_t/E of around 0.65. BESS has the lowest crop E_t/E with a value of 0.35. All datasets have similar forest E_t/E trend, with lowest mean E_t/E for DBF (0.54–0.69), followed by ENF (0.65–0.77). The highest mean E_t/E is exhibited for MF (0.61–0.90).

4.4 Sensitivity of E_t/E to f values

We perform a sensitivity analysis to investigate the effect of soil depth used in estimating f on the E_t/E values. Since $f = r_{10} \times S \times f_{AI}$, and both S and f_{AI} are constant for the watershed, differences in f arise from changes in r_{10}. Therefore, we tested the effect of using different depths of rapid response (5, 10, and 15 cm) on the resulting E_t/E values, which are shown in Fig. 8. We selected 5 and 10 cm based on the general consensus in the literature and extended the range to 15 cm to account for additional uncertainty. These depths represent plausible values for fast transpiration, and as discussed in Sect. 2.1, we do not consider larger depths to contribute significantly as fast transpiration.

The percentage and absolute changes in E_t/E resulting from variations in rapid response depth are summarized in Table 5 as average change per vegetation type (with six data products averaged for each type). The full results for individual data products are provided in Appendix A (Tables A1–A6). The largest percentage changes were observed for the grass type, with E_t/E varying by about 10 %–13 % when the depth was increased or decreased by 5 cm from the 10 cm reference. The largest absolute change occurred when the depth was increased from 5 to 15 cm for the ENF vegetation type, with a difference of 0.108. Overall, the differences due to changing the fast response depth are minor and remain well within the uncertainty ranges reported in the literature for evapotranspiration partitioning methods, as noted in the introduction.

5 Discussion

5.1 k and E_t/E ratios

Shrubs and grass showed higher k values, likely due to their occurrence in arid and semi-arid regions in the US. The high k values could be explained by the higher bare soil evaporation expected in arid regions (Baver et al., 1972), especially due to the sparse nature of shrubs, increasing bare areas and thus bare soil evaporation (Liu et al., 2022). Also, the high aridity is expected to cause water stress, lowering the continuing transpiration (portion of transpiration not included in k). The lower k values in crops and forests may be due to the higher vegetation coverage in these areas which provides shade to the soil, reducing the amount of soil evaporation (Baver et al., 1972). Additionally, litter contributes to reducing soil evaporation and may even have a larger reduction effect than canopy shade (Magliano et al., 2017). The broader leaves of DBF increase their interception compared to ENF, thus resulting in a higher k value as well.

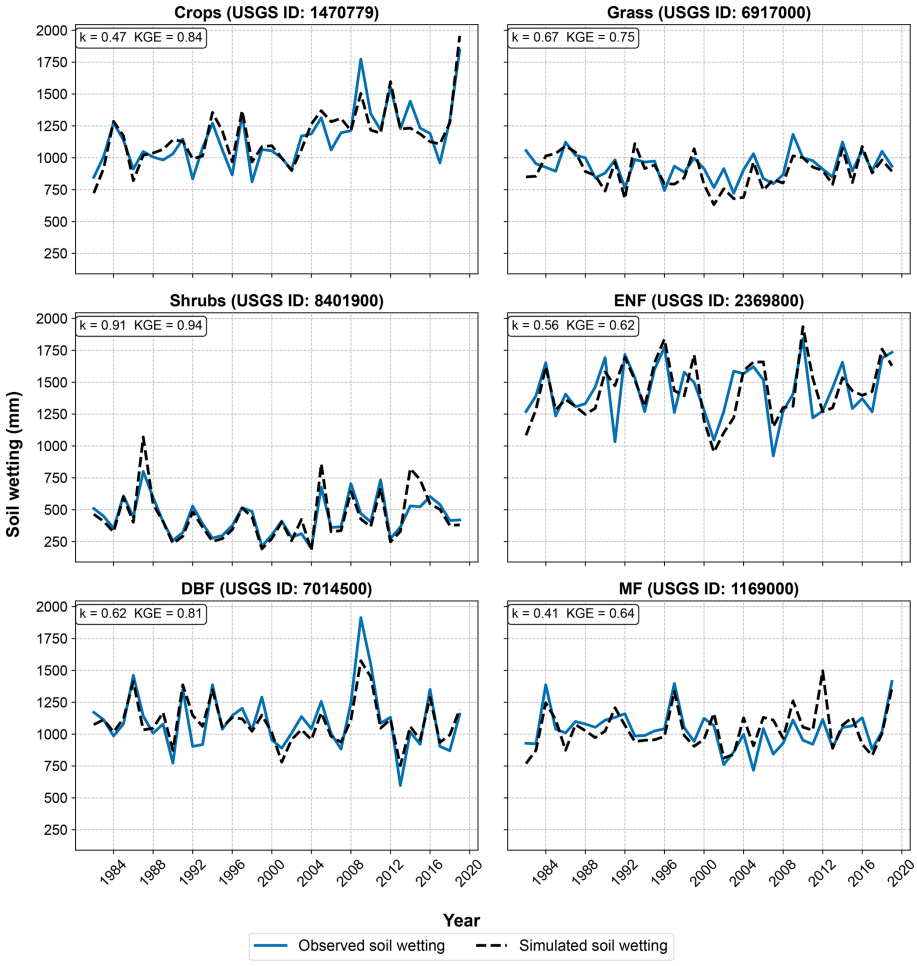

Figure 4. Optimization of k values using observed and simulated soil wetting as explained in Eqs. (5)–(7). Figure shows observed and simulated soil wetting time series for an example watershed for each of the six vegetation types (crops, grass, shrubs, ENF, DBF, MF) using NARR data.

Table 4. Mean E_t/E values for six vegetation types using E_p data from the six data products. Minimum, maximum, and mean values are shown for each vegetation type.

Data product	Crops	Grass	Shrubs	ENF	DBF	MF	Mean
NARR	0.52	0.37	0.37	0.72	0.59	0.61	0.52
MODIS	0.65	0.38	0.41	0.77	0.67	0.80	0.59
Zhang	0.49	0.34	0.34	0.69	0.69	0.90	0.52
GLEAM	0.48	0.28	0.31	0.67	0.54	0.67	0.48
SPLASH v2	0.43	0.30	0.29	0.65	0.55	0.71	0.47
BESS v2	0.35	0.25	0.30	0.65	0.56	0.64	0.45
Minimum	0.35	0.25	0.29	0.65	0.54	0.61	0.45
Maximum	0.65	0.38	0.41	0.77	0.69	0.90	0.59
Mean	0.48	0.32	0.33	0.69	0.60	0.70	0.50

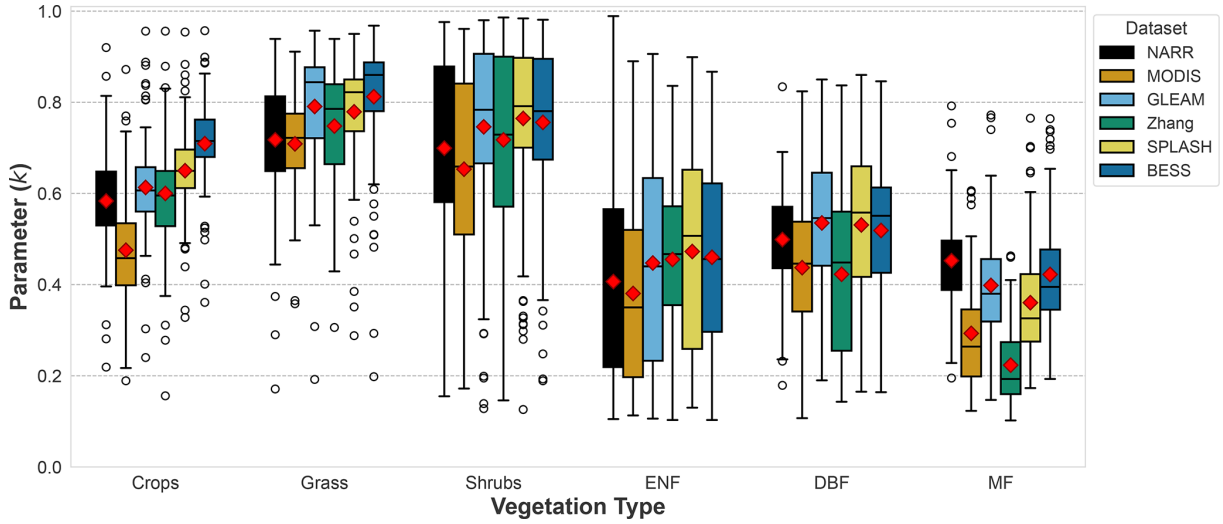

Figure 5. k values for the watersheds using data from six datasets: NARR, MODIS, Zhang et al. (2010), GLEAM after rescaling, SPLASH v2, and BESS v2. Note that ENF, DBF, and MF represent, respectively, evergreen needle-leaf forest, deciduous broadleaf forest, and mixed forest in the figure.

Table 5. Relative and absolute change in mean E_t/E values due to changes in fast transpiration depth. Results are shown as an average of the change in the six data products for each vegetation type.

Type	% Change in E_t/E			Absolute change in E_t/E		
	5 to 10 cm relative to 5 cm	10 to 15 cm relative to 10 cm	5 to 15 cm relative to 5 cm	5 to 10 cm	10 to 15 cm	5 to 15 cm
Crops	10.04	8.50	19.40	0.045	0.041	0.086
Grass	13.58	10.09	25.05	0.038	0.032	0.070
Shrubs	8.93	6.86	16.41	0.027	0.023	0.050
ENF	9.47	6.98	17.12	0.060	0.048	0.108
DBF	7.98	6.72	15.24	0.045	0.041	0.085
MF	5.49	4.52	10.26	0.038	0.033	0.071

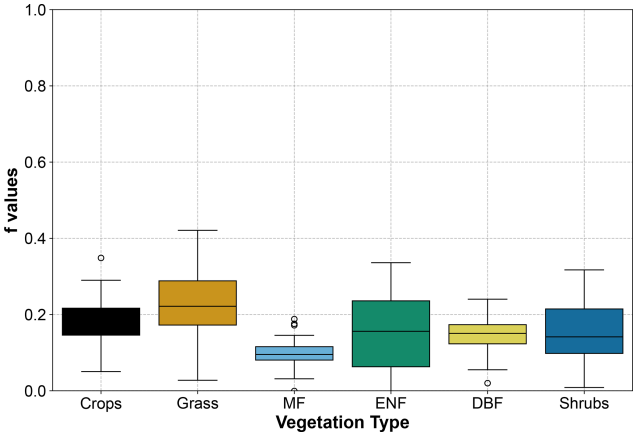

Figure 6. Portion of fast transpiration (f) values for the 648 watersheds classified into six vegetation types. ENF: evergreen needleleaf forest, DBF: deciduous broadleaf forest, MF: mixed forest.

These estimated mean E_t/E ratios followed explainable trends, with shrubs and grass watersheds showing low E_t/E ratios, forests exhibiting higher E_t/E ratios, and crops falling in between. Given greater water availability in crops and forests, it is expected that they would exhibit higher E_t/E ratios. Many crops in the US benefit from continuous irrigation, reducing water stress and promoting transpiration. Forests, with their dense canopy cover offering shade, reduce soil evaporation (Baver et al., 1972) and consequently boost the E_t/E ratios. Crops also show high vegetation coverage, thereby providing shade to the soil and increasing E_t/E (Baver et al., 1972). Moreover, in arid regions dominated by shrubs, lower soil water content is anticipated, resulting in diminished root water uptake (Gardner, 1983). Furthermore, the shedding of leaves in deciduous forests reduces transpiration when examined over the whole year (as here), resulting in a decreased E_t/E ratio for DBF.

Differences in study scale may hinder the comparison with other studies, since our method estimates E_t/E at the watershed scale, while other studies are based at a plot-scale (field/eddy covariance-based methods) or grid scale (mod-

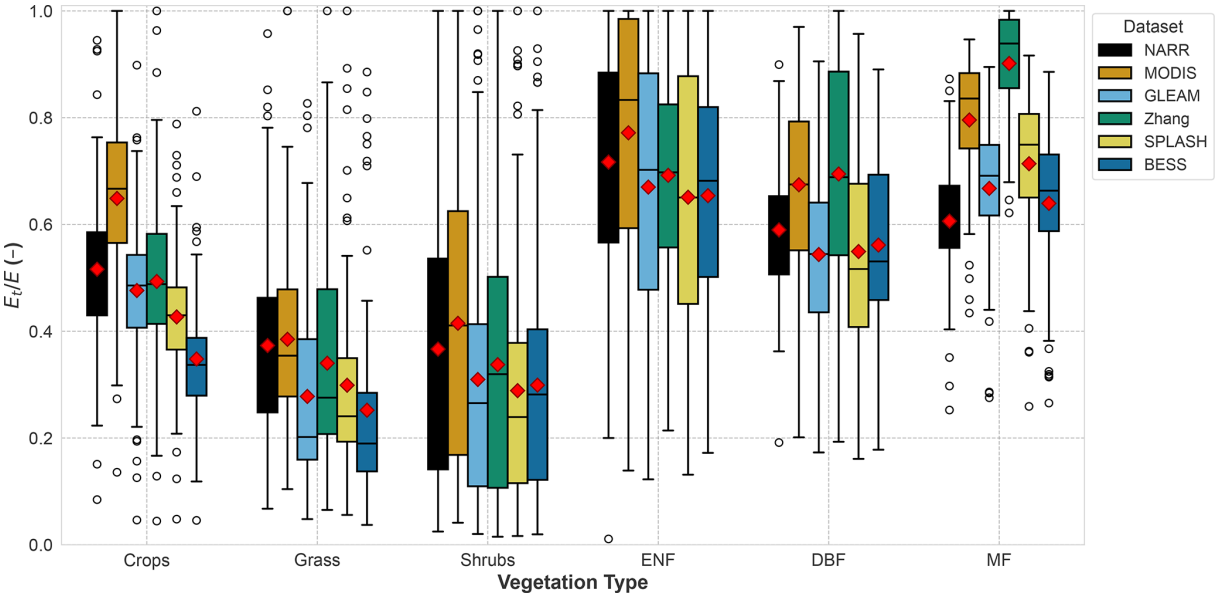

Figure 7. E_t/E values for the 648 watersheds using data from the six datasets: NARR, MODIS, Zhang et al. (2010), GLEAM after rescaling, SPLASH v2, and BESS v2.

els and remote-sensing methods). Factors affecting watershed scale E_t/E include the possible presence of secondary vegetation within the watershed and the possible sparseness of the primary vegetation and presence of bare areas which can increase soil evaporation and reduce E_t/E, especially for shrublands. Therefore, this method has the advantage of providing a realistic watershed E_t/E ratio that accounts for multiple vegetation types and sparseness in vegetation distribution. Consistent results across different datasets underscore the reliability of our new method, irrespective of the data product employed (see Fig. 7 and Table 4).

5.2 Effect of hydrological indices on E_t/E

We explore the sensitivity of E_t/E to two hydrological indices, namely the runoff ratio (Q/P) and the baseflow ratio (Q_b/Q). Figure 9a shows a proportional relationship between E_t/E and Q/P. The relationship appears to manifest as two distinct linear correlations, with arid catchments showing a steeper slope than humid catchments. Arid regions typically experience minimum runoff as a significant portion of precipitation evaporates in various forms owing to elevated atmospheric demand. This phenomenon yields high E_t/E ratios at relatively low Q/P values. Conversely, humid catchments often experience substantial runoff, attributed to either saturation excess or infiltration excess runoff mechanisms and the contribution of baseflow, resulting in elevated Q/P ratios compared to arid catchments at equivalent E_t/E values. In both cases, a higher Q/P ratio signifies increased water availability, consequently leading to higher E_t/E ratios.

In Fig. 9b a non-linear positive relationship is depicted between the mean E_t/E and Q_b/Q (baseflow ratio). The baseflow ratio serves as an indicator of soil water availability, as higher baseflow typically corresponds to increased soil moisture content (Hurkmans et al., 2008). Consequently, a positive correlation between E_t/E and the baseflow ratio is anticipated. Notably, the majority of arid catchments cluster in the low Q_b/Q and low E_t/E region, while transitioning toward wetter catchments naturally augments both Q_b/Q and E_t/E.

5.3 Effect of LAI on E_t/E

The leaf area index (LAI), representing the leaf area per unit ground area, reflects the combined influences of leaf size and canopy density. As shown in Fig. 10, LAI appears to exert some influence over evapotranspiration partitioning. Arid watersheds show lower LAI values, and E_t/E ratios increase non-linearly with LAI. However, as watersheds transition toward higher humidity levels, their LAI and E_t/E ratios increase non-linearly, albeit at different rates. In arid regions, plants tend to reduce their leaf area to mitigate water loss (Chaves et al., 2003) decreasing both LAI and E_t/E – a direct consequence of high aridity. This suggests that aridity plays a role in regulating E_t/E. Figure 10 illustrates a complex relationship between LAI and E_t/E, characterized by substantial scatter. Our findings align with previous studies indicating diverse dependence of E_t/E on LAI. For instance, LAI has been shown to provide a control on E partitioning (Li et al., 2019; Wang et al., 2014; Wei et al., 2017), but that effect varies from one study to another. Wang et al. (2014) showed that LAI has a non-linear relationship with E_t/E dur-

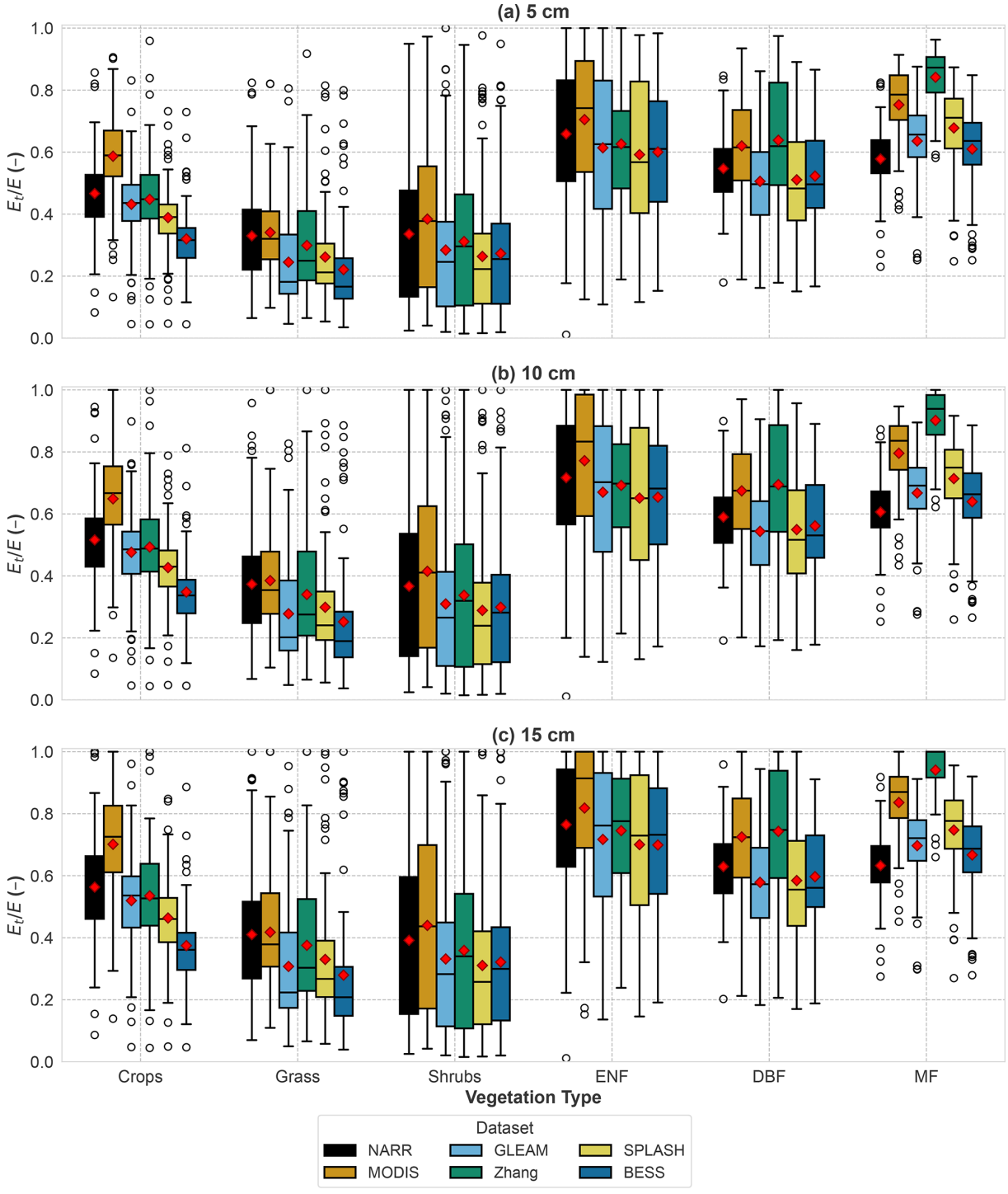

Figure 8. Sensitivity of E_t/E to different depths of fast transpiration responses: **(a)** 5 cm; **(b)** 10 cm; and **(c)** 15 cm.

ing the growing season, whereas Li et al. (2019) showed a weak linear relationship between mean growing season LAI and mean annual E_t/E across sites, with the E_t/E and LAI relationship within the same site being non-linear. Additionally, Cao et al. (2022) showed a non-linear positive relationship between annual E_t/E and LAI.

5.4 Impacts of environmental variables on E_t/E ratios

We explore the effect of six environmental factors on the mean E_t/E ratios. They are aridity index (AI), relative humidity (RH), air temperature (T_{air}), downward shortwave radiation (DSW), soil moisture, and wind speed (WS). These

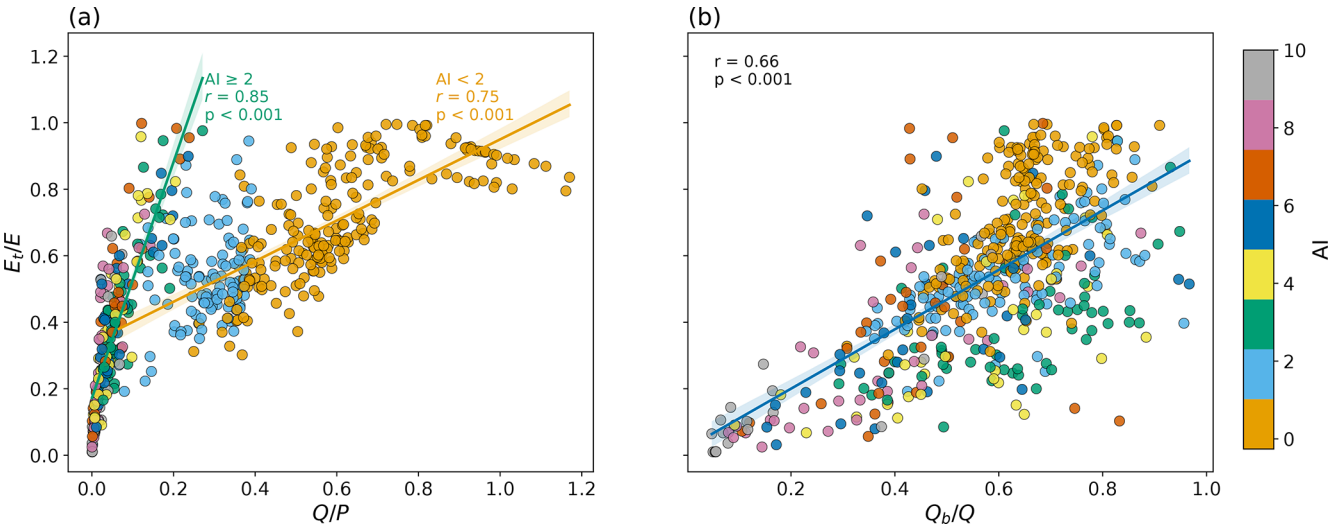

Figure 9. Relationship between mean E_t/E and two hydrological indices **(a)** Q/P and **(b)** Q_b/Q for 648 watersheds based on NARR data. Plots are colored according to aridity index.

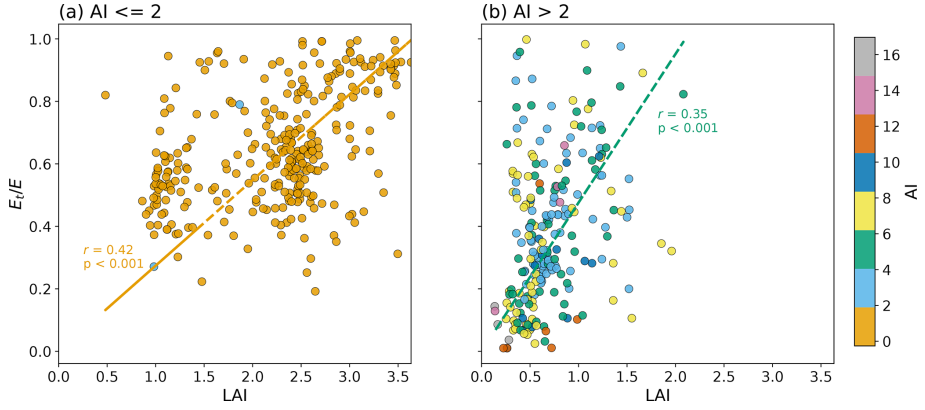

Figure 10. Relationship between E_t/E and LAI for 648 watersheds using E_t/E calculated based on the NARR dataset. **(a)** Aridity index (AI) less than or equal to 2; **(b)** AI greater than 2.

factors were derived from the NARR dataset, and the E_t/E ratios were calculated based on the same dataset. Since some of these environmental variables are highly correlated (as shown in Fig. 11), we first perform variable selection using stepwise regression and Lasso regression to identify those that are strongly correlated with each other. Stepwise regression aims to select a subset of variables that provide the best prediction with minimum redundancy, while Lasso regression adds a penalty term to reduce the coefficients of insignificant variables. Both methods resulted in the elimination of downward shortwave radiation, while stepwise selection additionally eliminated relative humidity and air temperature. Table 6 shows the coefficients of the environmental variables and their significance for both stepwise and Lasso regression. Although the significance test shows that air temperature and relative humidity have an insignificant impact on the Lasso regression, while the aridity index, soil moisture, and wind speed are significant (Table 6), they are still included because they marginally contribute to the model's predictive power. Additionally, they represent independent and observable dimensions, distinct from the other three significant environmental variables.

A negative non-linear correlation between E_t/E and AI is present (see Fig. 12a). Increased aridity prompts plants to adopt water conserving strategies (Chaves et al., 2003), thereby reducing the transpiration ratios. In humid regions, the relationship between E_t/E and AI is more discernible, with AI accounting for a significant portion of the variance of E_t/E. Conversely, for arid regions, particularly those dominated by shrubs, the relationship shows greater scatter, suggesting that AI exerts a relatively smaller effect on E_t/E, while other factors play a more prominent role. Furthermore, higher air temperature contributes to lowering E_t/E (see Fig. 12b), as it prompts water-conserving behaviors in

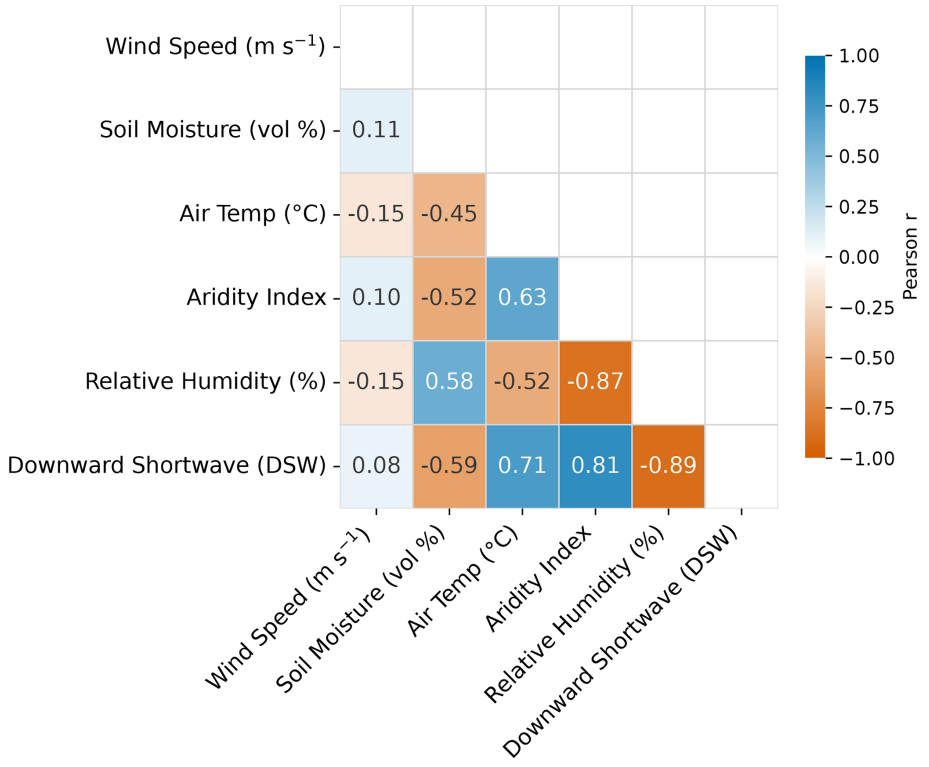

Figure 11. Correlation between environmental variables. AI: aridity index, RH: relative humidity, Ta: air temperature, DSW: downward shortwave radiation, SM: soil moisture, WS: wind speed.

Table 6. Coefficients of standardized environmental variables regressed against E_t/E using stepwise selection and Lasso regression. Significance levels are shown next to the coefficients (***: $p<0.001$, **: $p<0.01$, *: $p<0.05$, blank: $p>0.1$).

	Coefficient (Stepwise selection)	Coefficient (Lasso regression)
AI	−0.105***	−0.026***
RH		0.001
Tair		−0.004
DSW		
SM	0.066***	0.0005***
WS	0.023**	0.037*

plants and elevates soil evaporation, consequently reducing E_t/E ratios. Conversely, increasing soil moisture leads to enhanced water availability for plant root uptake, resulting in a near linear increase in E_t/E, as shown in Fig. 12c. The relationship between wind speed (WS) and E_t/E is inconclusive; this finding is consistent with several previous studies (Dixon and Grace, 1984; Huang et al., 2015; Schymanski and Or, 2016) which have presented a mixed effect of wind speed on transpiration. Nevertheless, the effects of other environmental variables on E_t/E demonstrate explainable patterns as discussed here. The other five data products (MODIS, Zhang, GLEAM, SPLASH, and BESS) show similar impacts of all the environmental variables on E_t/E as those shown in Fig. 12 for NARR.

5.5 E_t/P ratios

We computed transpiration to precipitation (E_t/P) ratios based on E_t/E values calculated from the six adjusted E_p data products. The mean E_t/P ratios from these six datasets range from 0.27 to 0.39, aligning closely with the global mean E_t/P of 0.39 estimated by Schlesinger and Jasechko (2014).

We also compared our estimated E_t/P ratios to the E_t/P versus aridity index relationship identified by Good et al. (2017). Good et al. (2017) presented this relationship based on a compilation of field studies, three remote-sensing based models, and an ecohydrological model, revealing good consistency among the various E_t/P data sources. Figure 13 shows a similar trend to that presented in Fig. 1 of Good et al. (2017), with the maximum E_t/P ratio close to the intersection between water and energy-limited states. This maximum E_t/P corresponds to an aridity index ranging between 2 and 3 in our study, similar to the estimated aridity index range of 1.3 to 1.9 for the maximum E_t/P as reported by Good et al. (2017). Moreover, the maximum E_t/P shown in Fig. 13 ranges between 0.52 and 0.59, consistent with the maximum E_t/P of 0.6 based on field data in Good et al. (2017). No-

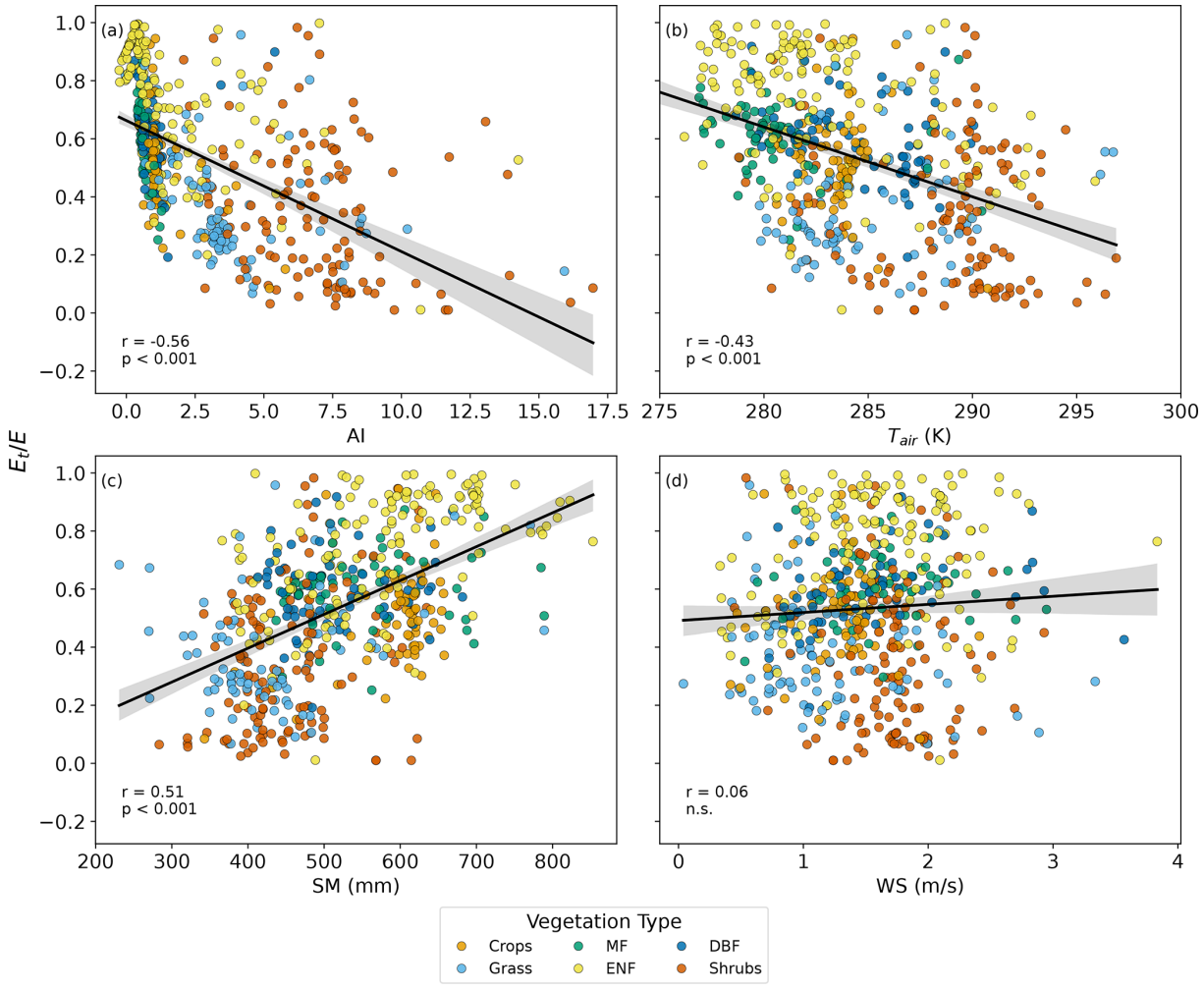

Figure 12. Relationships between mean annual E_t/E and environmental factors **(a)** aridity index (E_p/P), **(b)** air temperature (T_{air}), **(c)** soil moisture (SM), and **(d)** wind speed (WS) for 648 watersheds. E_t/E is calculated based on NARR data, and the environmental variables are also retrieved from the NARR product. Significance of the pairwise relationships between E_t/E and the environmental variables are shown on each plot.

tably, there is greater variation on the right side of the curve (indicating more arid conditions) compared to the left side (representing wetter conditions). In arid regions, transpiration is influenced not only by aridity, but also by factors such as groundwater table depth and soil moisture content, resulting in higher variability in the E_t/P versus aridity index (AI) relationship. The consistency between Good et al. (2017) and this study suggests that this relationship holds not only at the field and remote sensing scales (as shown by Good et al., 2017), but also at the watershed scale, as demonstrated in this study. This relationship holds significance for studies like that of Cai et al. (2025) and Zhou et al. (2025) where E_t/P serves as a parameter (referred to as f_0 in their study) to determine water-limited fAPAR and LAI. Cai et al. (2025) estimated E_t/P as a global mean using non-linear regression, with a value of 0.62, akin to the maximum E_t/P of 0.52 to 0.59 estimated by our fitted curves depicted in Fig. 13. Zhou et al. (2025) used a variable E_t/P as a function of AI, akin to our fitted curves. Their maximum E_t/P of 0.65 occurred at an AI of 1.9, similar to our fitted curves.

6 Variation of evapotranspiration partitioning methods

Figure 7 demonstrates the influence of the six adjusted E_p data products on the E_t/E ratios by our new method for each vegetation type, while Table 4 provides their variation range between the minimum and maximum mean E_t/E ratios. On the other hand, as outlined in the introduction, estimated global mean values of E_t/E from various existing methods exhibit a considerable variation, ranging from 0.24 to 0.9 (Liu et al., 2022; Wei et al., 2017). This variation may be attributed to several factors, including data inconsistencies, geographical disparities, and differences in selected

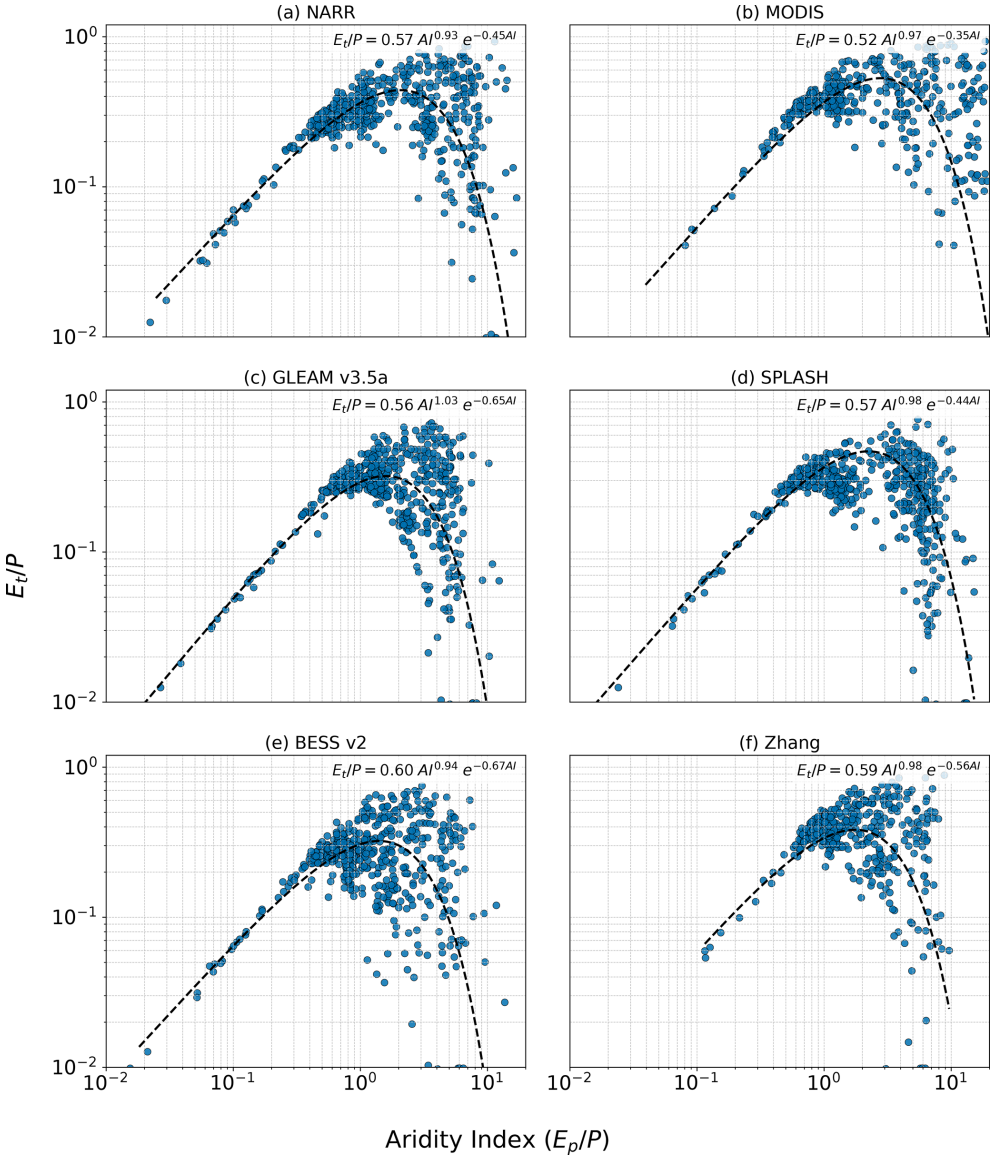

Figure 13. E_t/P versus the aridity index (AI) for six datasets: **(a)** NARR, **(b)** MODIS, **(c)** Zhang et al. (2010), **(d)** GLEAM after rescaling, **(e)** SPLASH v2, **(f)** BESS v2.

time periods, apart from differences in methodology. In an effort to explore what may be the cause for the large variation among the different methods, we have tried to mitigate these factors by using the same half-hourly eddy covariance data from the FLUXNET and AMERIFLUX ONEFLUX towers measurements in the US for the same locations and same time periods. Such an approach would allow us to elucidate the disparities among the existing E partitioning methods, consequently, providing insights on influences by different E_p datasets in our method versus current existing different methods on the large range of E_t/E ratios.

The four methods we selected to investigate are: (1) Zhou et al. (2016), (2) Scott and Biederman (2017), (3) Li et al. (2019), and (4) Yu et al. (2022). These four methods are selected because they are based on eddy covariance measurements whose data are widely available, unlike sap flow and isotope measurements. Since these methods are based on flux measurements, they can be considered as field-based estimations of E_t/E. We apply these four methods to the same datasets from the FLUXNET and AMERIFLUX ONEFLUX towers in the US, but the final number of flux towers included for each method depends on the filtering criteria in each method and the limitations in applying each method.

The first method by Zhou et al. (2016) is based on the water use efficiency. The ratio E_t/E is estimated as the ratio between the apparent water use efficiency ($WUE_a = GPP \times \frac{VPD^{0.5}}{ET}$) and the potential water use efficiency ($WUE_p =$

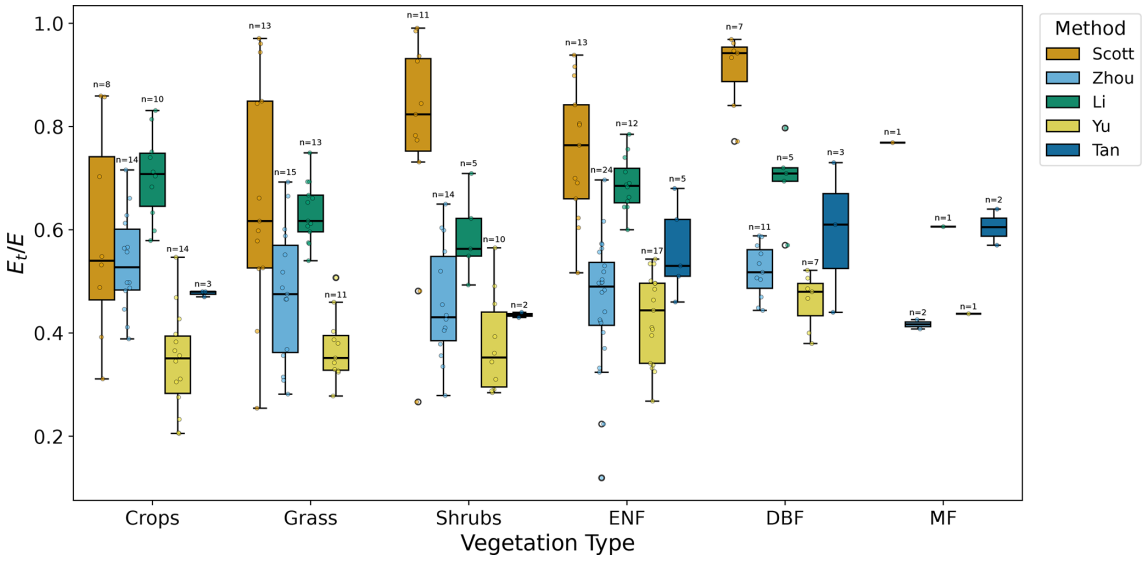

Figure 14. E_t/E values based on the eddy covariance tower data with 5 methods: Zhou et al. (2016) ($n = 80$), Scott and Biederman (2017) ($n = 53$), Li et al. (2019) ($n = 46$), Yu et al. (2022) (n =60) Tan et al. (2021) ($n = 15$).

GPP $\times \frac{\text{VPD}^{0.5}}{T}$). Assuming that E_t/E approaches 1 at some time during the growing season, the WUE_p is estimated from the 95th quantile regression of the half-hourly scatter plot (based on all half-hourly data for the site) between GPP $\times$ $\text{VPD}^{0.5}$ and E and is assumed to be constant for the flux tower. WUE_a is then estimated for each time step as the linear regression of the E and GPP $\times$ $\text{VPD}^{0.5}$ relationship using half-hourly data for the desired time period, which can be 8 d, monthly or annually.

The second method by Scott and Biederman (2017) is based on water use efficiency to estimate multiyear monthly average E_t/E ratios. This approach estimates transpiration as the product of the inverse of the marginal water use efficiency, the ratio between transpiration WUE and marginal WUE, and GPP. The inverse of the marginal WUE is estimated from the linear regression of the GPP versus E scatter plot. The ratio between transpirational and marginal WUEs is assumed to be 1. This method requires multiple years of data for its application.

The third method by Li et al. (2019) is based on the stomatal conductance model of Lin et al. (2018) to partition evapotranspiration. The E_t/E ratio is equivalent to the ratio between canopy conductance and ecosystem conductance. The eddy covariance data are divided into soil moisture bins to calibrate the parameters. Therefore, the method requires soil moisture data, along with GPP, VPD, E, and three calibrated parameters to estimate the E_t/E ratio.

The fourth method by Yu et al. (2022) combines the water use efficiency with the Medlyn et al. (2011) stomatal conductance model. This method relies on GPP, E, C_a, P_a, and VPD from the flux tower data in addition to the parameter g_1 from the Medlyn et al. (2011) model. The authors compared their method to other methods and showed a high correlation with the Zhou et al. (2016) but a low correlation with the Li et al. (2019) method.

Additionally, we compare our results to E_t/E values for 20 global flux towers used by Tan et al. (2021). E_t/E was calculated based on flux tower data and P-model (Stocker et al., 2020; Wang et al., 2017) outputs.

The estimated E_t/E ratios from the five methods are shown in Fig. 14 and Table 7, respectively, for the same six different vegetation types as shown in Fig. 7 with our new method.

The inconsistencies among the five methods are evident, with Zhou, Yu, Li, and Tan showing minimal variation among vegetation types, while Scott displays substantial variation. Moreover, the magnitudes and trends of E_t/E across these methods are also inconsistent. These discrepancies indicate a lack of agreement on both the mean E_t/E values and the variation ranges among the different methods. Consequently, these methods are not suitable as reference points for evaluating our new method. Instead, the assessment of our new method should be based on its physical behavior and relationships with other variables, as discussed in Sect. 5. It is noteworthy that compared to Fig. 7, the variation range of E_t/E ratios from the five different methods, utilizing the same data at the same locations, is significantly greater than that for our new method in which disparity is attributed to the variations associated with the E_p methods employed. Additionally, since our method is at a larger (watershed) scale, we observe larger variations between vegetation types, which can be attributed to different vegetation densities and bare land percentages at larger scales which is not a factor at smaller (flux tower) scales.

Table 7. Mean E_t/E values for six vegetation types using four evapotranspiration partitioning methods. Minimum, maximum, and mean values are shown for each vegetation type.

Evapotranspiration partitioning method	Crops	Grass	Shrubs	ENF	DBF	MF	Mean
Zhou et al. (2016)	0.54	0.48	0.46	0.46	0.52	0.42	0.48
Scott and Biederman (2017)	0.56	0.59	0.65	0.66	0.65	0.77	0.62
Li et al. (2019)	0.70	0.63	0.59	0.69	0.70	0.61	0.66
Yu et al. (2022)	0.34	0.37	0.38	0.43	0.46	0.44	0.39
Tan et al. (2021)	0.48	–	0.44	0.56	0.6	0.61	0.54
Minimum	0.34	0.37	0.38	0.43	0.46	0.42	0.39
Maximum	0.70	0.63	0.65	0.69	0.70	0.77	0.66
Mean	0.52	0.52	0.50	0.56	0.59	0.57	0.54

7 Conclusions

We have presented a new method for determining the transpiration to total evapotranspiration (E_t/E) ratio using long-term hydrological observations. This method is based on the generalized proportionality hypothesis, which has wide applications in hydrology. We applied the method to 648 watersheds in the US using six different E_p data products. Our findings demonstrate consistent E_t/E results across these diverse E_p datasets, facilitated by a rescaling of E_p derived from the E/E_p ratios obtained from each individual data product and watershed-budget estimated E computed from the watershed water balances.

Our analysis reveals that varying E_t/E ratios across watersheds are associated with different vegetation types, with shrubs and grasslands exhibiting lower E_t/E values compared to crops and forests. Furthermore, our results underscore the significant influence of leaf area index (LAI), hydrological indices (Q/P and Q_b/Q), and prevailing environmental conditions on E_t/E. Our method also provides a realistic estimate of E_t/E at a watershed scale that implicitly accounts for the heterogeneity of vegetation within the catchment. Our method can also be useful for constraining hydrological models, land surface models, and climate models.

We also explore the relationship between E_t/P and aridity index, unveiling a bell-shaped curve at the watershed scale, where the maximum E_t/P ratio occurs at an aridity index between 2 and 3, corresponding to an E_t/P ratio of around 0.52 to 0.59. These findings provide valuable insights into the intricate interplay between hydrological processes and environmental variables, shedding light on the complex dynamics of evapotranspiration in diverse watershed ecosystems.

Appendix A

Table A1. Relative and absolute change in mean E_t/E values due to changes in fast transpiration depth for the NARR dataset.

Type	% Change in E_t/E			Absolute change in E_t/E		
	5 to 10 cm relative to 5 cm	10 to 15 cm relative to 10 cm	5 to 15 cm relative to 5 cm	5 to 10 cm	10 to 15 cm	5to 15 cm
Crops	10.65	9.12	20.75	0.05	0.05	0.10
Grass	13.11	9.87	24.27	0.04	0.04	0.08
Shrubs	9.20	6.83	16.65	0.03	0.03	0.06
ENF	8.85	6.68	16.11	0.06	0.05	0.11
DBF	7.84	6.71	15.08	0.04	0.04	0.08
MF	4.91	4.33	9.45	0.03	0.03	0.05

Table A2. Relative and absolute change in mean E_t/E values due to changes in fast transpiration depth for the MODIS dataset.

Type	% Change in E_t/E			Absolute change in E_t/E		
	5 to 10 cm relative to 5 cm	10 to 15 cm relative to 10 cm	5 to 15 cm relative to 5 cm	5 to 10 cm	10 to 15 cm	5 to 15 cm
Crops	10.56	8.11	19.52	0.06	0.05	0.11
Grass	12.95	8.51	22.56	0.04	0.03	0.08
Shrubs	8.03	5.97	14.48	0.03	0.02	0.06
ENF	9.47	6.03	16.08	0.07	0.05	0.11
DBF	8.76	7.51	16.93	0.05	0.05	0.10
MF	5.73	5.07	11.09	0.04	0.04	0.08

Table A3. Relative and absolute change in mean E_t/E values due to changes in fast transpiration depth for the GLEAM dataset.

Type	% Change in E_t/E			Absolute change in E_t/E		
	5 to 10 cm relative to 5 cm	10 to 15 cm relative to 10 cm	5 to 15 cm relative to 5 cm	5 to 10 cm	10 to 15 cm	5 to 15 cm
Crops	10.31	9.11	20.36	0.04	0.04	0.09
Grass	13.42	10.58	25.43	0.03	0.03	0.06
Shrubs	9.00	7.05	16.68	0.03	0.02	0.05
ENF	9.13	7.01	16.77	0.06	0.05	0.10
DBF	7.52	6.40	14.40	0.04	0.03	0.07
MF	4.99	4.40	9.62	0.03	0.03	0.06

Table A4. Relative and absolute change in mean E_t/E values due to changes in fast transpiration depth for the Zhang dataset.

Type	% Change in E_t/E			Absolute change in E_t/E		
	5 to 10 cm relative to 5 cm	10 to 15 cm relative to 10 cm	5 to 15 cm relative to 5 cm	5 to 10 cm	10 to 15 cm	5 to 15 cm
Crops	10.20	8.48	19.54	0.05	0.04	0.09
Grass	13.73	10.39	25.54	0.04	0.04	0.08
Shrubs	8.29	6.35	15.16	0.03	0.02	0.05
ENF	10.50	7.70	19.01	0.07	0.05	0.12
DBF	8.80	6.98	16.40	0.06	0.05	0.10
MF	7.13	4.33	11.77	0.06	0.04	0.10

Table A5. Relative and absolute change in mean E_t/E values due to changes in fast transpiration depth for the SPLASH v2 dataset.

Type	% Change in E_t/E			Absolute change in E_t/E		
	5 to 10 cm relative to 5 cm	10 to 15 cm relative to 10 cm	5 to 15 cm relative to 5 cm	5 to 10 cm	10 to 15 cm	5 to 15 cm
Crops	9.78	8.60	19.22	0.04	0.04	0.07
Grass	14.23	10.40	26.11	0.04	0.03	0.07
Shrubs	9.56	7.53	17.82	0.03	0.02	0.05
ENF	9.99	7.57	18.32	0.06	0.05	0.11
DBF	7.56	6.39	14.43	0.04	0.04	0.07
MF	5.29	4.68	10.23	0.04	0.03	0.07

Table A6. Relative and absolute change in mean E_t/E values due to changes in fast transpiration depth for the BESS v2 dataset.

Type	% Change in E_t/E			Absolute change in E_t/E		
	5 to 10 cm relative to 5 cm	10 to 15 cm relative to 10 cm	5 to 15 cm relative to 5 cm	5 to 10 cm	10 to 15 cm	5 to 15 cm
Crops	8.76	7.61	17.04	0.03	0.03	0.05
Grass	14.06	10.80	26.38	0.03	0.03	0.06
Shrubs	9.50	7.46	17.68	0.03	0.02	0.05
ENF	8.90	6.89	16.41	0.05	0.05	0.10
DBF	7.40	6.33	14.19	0.04	0.04	0.07
MF	4.87	4.29	9.37	0.03	0.03	0.06

Data availability. Streamflow observations were obtained from the U.S. Geological Survey (USGS) National Water Information System. Watershed boundaries and precipitation were retrieved from the HYSETS dataset (https://doi.org/10.17605/OSF.IO/RPC3W, Arsenault et al., 2024). Land cover information was obtained from the ESA Climate Change Initiative (CCI) Land Cover project (https://www.esa-landcover-cci.org/, last access: 28 December 2022). Potential evapotranspiration data were obtained from six publicly available data products: NARR (https://psl.noaa.gov/data/gridded/data.narr.html, last access: 5 October 2022), MODIS MOD16A3GF (https://lpdaac.usgs.gov/, last access: 5 October 2022), GLEAM v3.5a (https://www.gleam.eu/, last access: 4 October 2022), SPLASH v2.0 (https://github.com/dsval/rsplash, last access: 18 December 2025; DOI: https://doi.org/10.5281/zenodo.10047627, Sandoval, 2023), BESS v2 (https://www.environment.snu.ac.kr/bessv2, last access: 4 September 2023), and the dataset of Zhang et al. (2010). Meteorological data and soil moisture were obtained from NARR. Root distribution parameters were taken from Zeng (2001). Leaf area index data were obtained from the Global Monthly Mean Leaf Area Index Climatology provided by ORNL DAAC (https://daac.ornl.gov/, last access: 4 March 2020). Baseflow was derived from USGS streamflow data using the Web-based Hydrological Analysis Tool (WHAT; https://app.envsys.co.kr/what2020/, last access: 18 December 2025). All datasets used in this study are publicly available from the sources listed above.

Author contributions. AH implemented the research ideas, designed and performed the experiments, analyzed the results, drafted the manuscript. XL conceived the research ideas, designed the experiments, analyzed the results, supervised the investigation, and wrote and finalized the manuscript. ICP initiated the research topic, analyzed the results, edited the manuscript.

Competing interests. The contact author has declared that none of the authors has any competing interests.

Disclaimer. Publisher's note: Copernicus Publications remains neutral with regard to jurisdictional claims made in the text, published maps, institutional affiliations, or any other geographical representation in this paper. The authors bear the ultimate responsibility for providing appropriate place names. Views expressed in the text are those of the authors and do not necessarily reflect the views of the publisher.

Acknowledgements. The authors would like to thank Wenjia Cai for providing the SPLASH v2 model datasets, and Youngryel Ryu and Xing Li for providing the BESS v2 PET dataset.

Financial support. This work was supported by Schmidt Sciences through the LEMONTREE (Land Ecosystem Models based On New Theory, obseRvations and ExperimEnts) project.

Review statement. This paper was edited by Miriam Coenders-Gerrits and reviewed by Stephen Good and one anonymous referee.

References

Abeshu, G. W. and Li, H. Y.: Horton Index: Conceptual Framework for Exploring Multi-Scale Links Between Catchment Water Bal-

ance and Vegetation Dynamics, Water Resources Research, 57, https://doi.org/10.1029/2020WR029343, 2021.

Abolafia-Rosenzweig, R., Badger, A. M., Small, E. E., and Livneh, B.: A continental-scale soil evaporation dataset derived from Soil Moisture Active Passive satellite drying rates, Scientific Data, 7, 1–10, https://doi.org/10.1038/s41597-020-00748-z, 2020.

Alemohammad, S. H., Fang, B., Konings, A. G., Aires, F., Green, J. K., Kolassa, J., Miralles, D., Prigent, C., and Gentine, P.: Water, Energy, and Carbon with Artificial Neural Networks (WECANN): a statistically based estimate of global surface turbulent fluxes and gross primary productivity using solar-induced fluorescence, Biogeosciences, 14, 4101–4124, https://doi.org/10.5194/bg-14-4101-2017, 2017.

Arsenault, R., Brissette, F., Martel, J. L., Troin, M., Lévesque, G., Davidson-Chaput, J., Gonzalez, M. C., Ameli, A., and Poulin, A.: A comprehensive, multisource database for hydrometeorological modeling of 14,425 North American watersheds, Scientific Data, 7, https://doi.org/10.1038/s41597-020-00583-2, 2020.

Arsenault, R., Brissette, F., Martel, J., et al.: HYSETS – A 14425 watershed Hydrometeorological Sandbox over North America, OSF [data set], https://doi.org/10.17605/OSF.IO/RPC3W, 2024.

Baver, L. D., Gardner, W. H., and Gardner, W. R.: Soil Physics, John Wiley & Sons, New York, ISBN 0471059749, 1972.

Berkelhammer, M., Noone, D. C., Wong, T. E., Burns, S. P., Knowles, J. F., Kaushik, A., Blanken, P. D., and Williams, M. W.: Convergent approaches to determine an ecosystem's transpiration fraction, Global Biogeochemical Cycles, 30, 933–951, https://doi.org/10.1002/2016GB005392, 2016.

Cai, W., Zhu, Z., Harrison, S. P., Ryu, Y., Wang, H., Zhou, B., and Prentice, I. C.: A unifying principle for global greenness patterns and trends, Commun. Earth Environ., 6, 19, https://doi.org/10.1038/s43247-025-01992-0, 2025.

Cao, R., Huang, H., Wu, G., Han, D., Jiang, Z., Di, K., and Hu, Z.: Spatiotemporal variations in the ratio of transpiration to evapotranspiration and its controlling factors across terrestrial biomes, Agricultural and Forest Meteorology, 321, https://doi.org/10.1016/j.agrformet.2022.108984, 2022.

Cavanaugh, M. L., Kurc, S. A., and Scott, R. L.: Evapotranspiration partitioning in semiarid shrubland ecosystems: a two-site evaluation of soil moisture control on transpiration, Ecohydrology, 4, 671–681, https://doi.org/10.1002/ECO.157, 2011.

Čermák, J., Deml, M., and Penka, M.: A new method of sap flow rate determination in trees, Biologia Plantarum, 15, 171–178, https://doi.org/10.1007/BF02922390, 1973.

Čermák, J., Kučera, J., and Nadezhdina, N.: Sap flow measurements with some thermodynamic methods, flow integration within trees and scaling up from sample trees to entire forest stands, Trees, 18, 529–546, https://doi.org/10.1007/S00468-004-0339-6, 2004.

Chaves, M. M., Maroco, J. P., and Pereira, J. S.: Understanding plant responses to drought – from genes to the whole plant, Functional Plant Biology, 30, 239, https://doi.org/10.1071/FP02076, 2003.

Chen, X. and Wang, D.: Modeling seasonal surface runoff and base flow based on the generalized proportionality hypothesis, Journal of Hydrology, 527, 367–379, https://doi.org/10.1016/j.jhydrol.2015.04.059, 2015.

Cohen, Y., Fuchs, M., and Green, G. C.: Improvement of the heat pulse method for determining sap flow in trees, Plant, Cell & Environment, 4, 391–397, https://doi.org/10.1111/J.1365-3040.1981.TB02117.X, 1981.

Damm, A., Roethlin, S., and Fritsche, L.: Towards advanced retrievals of plant transpiration using suninduced chlorophyll fluorescence: First considerations, International Geoscience and Remote Sensing Symposium (IGARSS), July 2018, 5983–5986, https://doi.org/10.1109/IGARSS.2018.8518974, 2018.

Dixon, M. and Grace, J.: Effect of Wind on the Transpiration of Young Trees, Annals of Botany, 53, 811–819, https://doi.org/10.1093/oxfordjournals.aob.a086751, 1984.

Eckhardt, K.: How to construct recursive digital filters for baseflow separation, Hydrological Processes, 19, 507–515, https://doi.org/10.1002/hyp.5675, 2005.

Eckhardt, K.: A comparison of baseflow indices, which were calculated with seven different baseflow separation methods, Journal of Hydrology, 352, 168–173, https://doi.org/10.1016/J.JHYDROL.2008.01.005, 2008.

Fan, J., McConkey, B., Wang, H., and Janzen, H.: Root distribution by depth for temperate agricultural crops, Field Crops Research, 189, 68–74, https://doi.org/10.1016/j.fcr.2016.02.013, 2016.

Gardner, W. R.: Soil Properties and Efficient Water Use: An Overview, in: Limitations to Efficient Water Use in Crop Production, 45–64, https://doi.org/10.2134/1983.limitationstoefficientwateruse.c3, 1983.

Gerrits, A. M. J., Savenije, H. H. G., Veling, E. J. M., and Pfister, L.: Analytical derivation of the Budyko curve based on rainfall characteristics and a simple evaporation model, Water Resources Research, 45, https://doi.org/10.1029/2008WR007308, 2009.

Good, S. P., Moore, G. W., and Miralles, D. G.: A mesic maximum in biological water use demarcates biome sensitivity to aridity shifts, Nature Ecology and Evolution, 1, 1883–1888, https://doi.org/10.1038/s41559-017-0371-8, 2017.

Granier, A.: Une nouvelle méthode pour la mesure du flux de sève brute dans le tronc des arbres, Annales des Sciences Forestières, 42, 193–200, https://doi.org/10.1051/forest:19850204, 1985.

Green, J. K., Zhang, Y., Luo, X., and Keenan, T. F.: Systematic Underestimation of Canopy Conductance Sensitivity to Drought by Earth System Models, AGU Advances, 5, https://doi.org/10.1029/2023AV001026, 2024.

Green, S., Clothier, B., and Jardine, B.: Theory and Practical Application of Heat Pulse to Measure Sap Flow, Agronomy Journal, 95, 1371–1379, https://doi.org/10.2134/agronj2003.1371, 2003.

Griffis, T. J.: Tracing the flow of carbon dioxide and water vapor between the biosphere and atmosphere: A review of optical isotope techniques and their application, Agricultural and Forest Meteorology, 174–175, 85–109, https://doi.org/10.1016/J.AGRFORMET.2013.02.009, 2013.

Gupta, H. V., Kling, H., Yilmaz, K. K., and Martinez, G. F.: Decomposition of the mean squared error and NSE performance criteria: Implications for improving hydrological modelling, Journal of Hydrology, 377, 80–91, https://doi.org/10.1016/j.jhydrol.2009.08.003, 2009.

Hall, A., Cox, P., Huntingford, C., and Klein, S.: Progressing emergent constraints on future climate change, Nature Climate Change, 9, 269–278, https://doi.org/10.1038/s41558-019-0436-6, 2019.

Hassan, A., Prentice, I. C., and Liang, X.: Understanding the Variability in Potential Evapotranspiration (PET) Products for U.S. Watersheds, in: AGU24, 9–13 December 2024, https://agu.

confex.com/agu/agu24/meetingapp.cgi/Paper/1599970, last access: 13 December 2024.

Huang, C.-W., Chu, C.-R., Hsieh, C.-I., Palmroth, S., and Katul, G. G.: Wind-induced leaf transpiration, Advances in Water Resources, 86, 240–255, https://doi.org/10.1016/j.advwatres.2015.10.009, 2015.

Hurkmans, R. T. W. L., De Moel, H., Aerts, J. C. J. H., and Troch, P. A.: Water balance versus land surface model in the simulation of Rhine river discharges, Water Resources Research, 44, https://doi.org/10.1029/2007WR006168, 2008.

Jackson, R. B., Canadell, J., Ehleringer, J. R., Mooney, H. A., Sala, O. E., and Schulze, E. D.: A global analysis of root distributions for terrestrial biomes, Oecologia, 108, 389–411, https://doi.org/10.1007/BF00333714, 1996.

Kool, D., Agam, N., Lazarovitch, N., Heitman, J. L., Sauer, T. J., and Ben-Gal, A.: A review of approaches for evapotranspiration partitioning, Agricultural and Forest Meteorology, 184, 56–70, https://doi.org/10.1016/j.agrformet.2013.09.003, 2014.

L'Vovich, M. I.: World water resources and their future, American Geophysical Union, 415 pp., https://doi.org/10.1029/SP013, 1979.

Li, B., Ryu, Y., Jiang, C., Dechant, B., Liu, J., Yan, Y., and Li, X.: BESSv2.0: A satellite-based and coupled-process model for quantifying long-term global land–atmosphere fluxes, Remote Sensing of Environment, 295, https://doi.org/10.1016/j.rse.2023.113696, 2023.

Li, M., Wu, P., Ma, Z., Pan, Z., Lv, M., Yang, Q., and Duan, Y.: The Increasing Role of Vegetation Transpiration in Soil Moisture Loss across China under Global Warming, Journal of Hydrometeorology, 23, 253–274, https://doi.org/10.1175/JHM-D-21-0132.1, 2022.

Li, X., Gentine, P., Lin, C., Zhou, S., Sun, Z., Zheng, Y., Liu, J., and Zheng, C.: A simple and objective method to partition evapotranspiration into transpiration and evaporation at eddy-covariance sites, Agricultural and Forest Meteorology, 265, 171–182, https://doi.org/10.1016/J.AGRFORMET.2018.11.017, 2019.

Lim, K. J., Engel, B. A., Tang, Z., Choi, J., Kim, K. S., Muthukrishnan, S., and Tripathy, D.: Automated Web GIS Based Hydrograph Analysis Tool, WHAT, JAWRA Journal of the American Water Resources Association, 41, 1407–1416, https://doi.org/10.1111/J.1752-1688.2005.TB03808.X, 2005.

Lim, K. J., Park, Y. S., Kim, J., Shin, Y. C., Kim, N. W., Kim, S. J., Jeon, J. H., and Engel, B. A.: Development of genetic algorithm-based optimization module in WHAT system for hydrograph analysis and model application, Computers & Geosciences, 36, 936–944, https://doi.org/10.1016/J.CAGEO.2010.01.004, 2010.

Lin, C., Gentine, P., Huang, Y., Guan, K., Kimm, H., and Zhou, S.: Diel ecosystem conductance response to vapor pressure deficit is suboptimal and independent of soil moisture, Agricultural and Forest Meteorology, 250–251, 24–34, https://doi.org/10.1016/J.AGRFORMET.2017.12.078, 2018.

Liu, Y., Zhang, Y., Shan, N., Zhang, Z., and Wei, Z.: Global assessment of partitioning transpiration from evapotranspiration based on satellite solar-induced chlorophyll fluorescence data, Journal of Hydrology, 612, 128044, https://doi.org/10.1016/J.JHYDROL.2022.128044, 2022.

Lozanova, L., Zhiyanski, M., Vanguelova, E., Doncheva, S., Marinov, M. P., and Lazarova, S.: Dynamics and Vertical Distribution of Roots in European Beech Forests and Douglas Fir Plantations in Bulgaria, Forests 2019, 10, 1123, https://doi.org/10.3390/F10121123, 2019.

Lu, X., Liu, Z., An, S., Miralles, D. G., Maes, W., Liu, Y., and Tang, J.: Potential of solar-induced chlorophyll fluorescence to estimate transpiration in a temperate forest, Agricultural and Forest Meteorology, 252, 75–87, https://doi.org/10.1016/J.AGRFORMET.2018.01.017, 2018.

Lyne, V. and Hollick, M.: Stochastic time-variable rainfall-runoff modelling, in: Institute of engineers Australia national conference, 89–93, https://www.researchgate.net/profile/Vincent-Lyne/publication/272491803_Stochastic_Time-Variable_Rainfall-Runoff_Modeling/links/54f45fb40cf299c8d9e6e6c1/Stochastic-Time-Variable-Rainfall-Runoff-Modeling.pdf (last access: 8 May 2025), 1979.

Magliano, P. N., Giménez, R., Houspanossian, J., Páez, R. A., Nosetto, M. D., Fernández, R. J., and Jobbágy, E. G.: Litter is more effective than forest canopy reducing soil evaporation in Dry Chaco rangelands, Ecohydrology, 10, https://doi.org/10.1002/eco.1879, 2017.

Mao, J. and Yan, B.: Global Monthly Mean Leaf Area Index Climatology, 1981–2015, ORNL Distributed Active Archive Center [data set], https://doi.org/10.3334/ORNLDAAC/1653, 2019.

Martens, B., Miralles, D. G., Lievens, H., van der Schalie, R., de Jeu, R. A. M., Fernández-Prieto, D., Beck, H. E., Dorigo, W. A., and Verhoest, N. E. C.: GLEAM v3: satellite-based land evaporation and root-zone soil moisture, Geosci. Model Dev., 10, 1903–1925, https://doi.org/10.5194/gmd-10-1903-2017, 2017.

Medlyn, B. E., Duursma, R. A., Eamus, D., Ellsworth, D. S., Prentice, I. C., Barton, C. V. M., Crous, K. Y., De Angelis, P., Freeman, M., and Wingate, L.: Reconciling the optimal and empirical approaches to modelling stomatal conductance, Global Change Biology, 17, 2134–2144, https://doi.org/10.1111/J.1365-2486.2010.02375.X, 2011.

Mesinger, F., DiMego, G., Kalnay, E., Mitchell, K., Shafran, P. C., Ebisuzaki, W., Jović, D., Woollen, J., Rogers, E., Berbery, E. H., Ek, M. B., Fan, Y., Grumbine, R., Higgins, W., Li, H., Lin, Y., Manikin, G., Parrish, D., and Shi, W.: North American Regional Reanalysis, Bulletin of the American Meteorological Society, 87, 343–360, https://doi.org/10.1175/BAMS-87-3-343, 2006.

Mianabadi, A., Coenders-Gerrits, M., Shirazi, P., Ghahraman, B., and Alizadeh, A.: A global Budyko model to partition evaporation into interception and transpiration, Hydrol. Earth Syst. Sci., 23, 4983–5000, https://doi.org/10.5194/hess-23-4983-2019, 2019.

Moran, M. S., Scott, R. L., Keefer, T. O., Emmerich, W. E., Hernandez, M., Nearing, G. S., Paige, G. B., Cosh, M. H., and O'Neill, P. E.: Partitioning evapotranspiration in semiarid grassland and shrubland ecosystems using time series of soil surface temperature, Agricultural and Forest Meteorology, 149, 59–72, https://doi.org/10.1016/J.AGRFORMET.2008.07.004, 2009.

Niu, Z., He, H., Zhu, G., Ren, X., Zhang, L., Zhang, K., Yu, G., Ge, R., Li, P., Zeng, N., and Zhu, X.: An increasing trend in the ratio of transpiration to total terrestrial evapotranspiration in China from 1982 to 2015 caused by greening and warming, Agricultural and Forest Meteorology, 279, https://doi.org/10.1016/j.agrformet.2019.107701, 2019.

Pagán, B. R., Maes, W. H., Gentine, P., Martens, B., and Miralles, D. G.: Exploring the Potential of Satellite Solar-Induced Fluo-

rescence to Constrain Global Transpiration Estimates, Remote Sensing, 11, 413, https://doi.org/10.3390/RS11040413, 2019.

Peng, L., Zeng, Z., Wei, Z., Chen, A., Wood, E. F., and Sheffield, J.: Determinants of the ratio of actual to potential evapotranspiration, Global Change Biology, 25, 1326–1343, https://doi.org/10.1111/gcb.14577, 2019.

Ponce, V. M. and Shetty, A. V.: A conceptual model of catchment water balance: 1. Formulation and calibration, Journal of Hydrology, 173, 27–40, https://doi.org/10.1016/0022-1694(95)02739-C, 1995a.

Ponce, V. M. and Shetty, A. V.: A conceptual model of catchment water balance: 2. Application to runoff and baseflow modeling, Journal of Hydrology, 173, 41–50, https://doi.org/10.1016/0022-1694(95)02745-B, 1995b.

Pool, S., Vis, M., and Seibert, J.: Evaluating model performance: towards a non-parametric variant of the Kling-Gupta efficiency, Hydrological Sciences Journal, 63, 1941–1953, https://doi.org/10.1080/02626667.2018.1552002, 2018.

Poyatos, R., Granda, V., Flo, V., Adams, M. A., Adorján, B., Aguadé, D., Aidar, M. P. M., Allen, S., Alvarado-Barrientos, M. S., Anderson-Teixeira, K. J., Aparecido, L. M., Arain, M. A., Aranda, I., Asbjornsen, H., Baxter, R., Beamesderfer, E., Berry, Z. C., Berveiller, D., Blakely, B., Boggs, J., Bohrer, G., Bolstad, P. V., Bonal, D., Bracho, R., Brito, P., Brodeur, J., Casanoves, F., Chave, J., Chen, H., Cisneros, C., Clark, K., Cremonese, E., Dang, H., David, J. S., David, T. S., Delpierre, N., Desai, A. R., Do, F. C., Dohnal, M., Domec, J.-C., Dzikiti, S., Edgar, C., Eichstaedt, R., El-Madany, T. S., Elbers, J., Eller, C. B., Euskirchen, E. S., Ewers, B., Fonti, P., Forner, A., Forrester, D. I., Freitas, H. C., Galvagno, M., Garcia-Tejera, O., Ghimire, C. P., Gimeno, T. E., Grace, J., Granier, A., Griebel, A., Guangyu, Y., Gush, M. B., Hanson, P. J., Hasselquist, N. J., Heinrich, I., Hernandez-Santana, V., Herrmann, V., Hölttä, T., Holwerda, F., Irvine, J., Isarangkool Na Ayutthaya, S., Jarvis, P. G., Jochheim, H., Joly, C. A., Kaplick, J., Kim, H. S., Klemedtsson, L., Kropp, H., Lagergren, F., Lane, P., Lang, P., Lapenas, A., Lechuga, V., Lee, M., Leuschner, C., Limousin, J.-M., Linares, J. C., Linderson, M.-L., Lindroth, A., Llorens, P., López-Bernal, Á., Loranty, M. M., Lüttschwager, D., Macinnis-Ng, C., Maréchaux, I., Martin, T. A., Matheny, A., McDowell, N., McMahon, S., Meir, P., Mészáros, I., Migliavacca, M., Mitchell, P., Mölder, M., Montagnani, L., Moore, G. W., Nakada, R., Niu, F., Nolan, R. H., Norby, R., Novick, K., Oberhuber, W., Obojes, N., Oishi, A. C., Oliveira, R. S., Oren, R., Ourcival, J.-M., Paljakka, T., Perez-Priego, O., Peri, P. L., Peters, R. L., Pfautsch, S., Pockman, W. T., Preisler, Y., Rascher, K., Robinson, G., Rocha, H., Rocheteau, A., Röll, A., Rosado, B. H. P., Rowland, L., Rubtsov, A. V., Sabaté, S., Salmon, Y., Salomón, R. L., Sánchez-Costa, E., Schäfer, K. V. R., Schuldt, B., Shashkin, A., Stahl, C., Stojanović, M., Suárez, J. C., Sun, G., Szatniewska, J., Tatarinov, F., Tesař, M., Thomas, F. M., Tor-ngern, P., Urban, J., Valladares, F., van der Tol, C., van Meerveld, I., Varlagin, A., Voigt, H., Warren, J., Werner, C., Werner, W., Wieser, G., Wingate, L., Wullschleger, S., Yi, K., Zweifel, R., Steppe, K., Mencuccini, M., and Martínez-Vilalta, J.: Global transpiration data from sap flow measurements: the SAPFLUXNET database, Earth Syst. Sci. Data, 13, 2607–2649, https://doi.org/10.5194/essd-13-2607-2021, 2021.

Running, S., Mu, Q., Zhao, M., and Moreno, A.: MODIS/Terra Net Evapotranspiration Gap-Filled Yearly L4 Global 500m SIN Grid V061, NASA Land Processes Distributed Active Archive Center [data set], https://doi.org/10.5067/MODIS/MOD16A3GF.061, 2022.

Sakuratani, T.: A Heat Balance Method for Measuring Water Flux in the Stem of Intact Plants, Journal of Agricultural Meteorology, 37, 9–17, https://doi.org/10.2480/AGRMET.37.9, 1981.

Sakuratani, T.: Studies on Evapotranspiration from Crops (2) Separate Estimation of Transpiration and Evaporation from a Soybean Field without Water Shortage, Journal of Agricultural Meteorology, 42, 309–317, https://doi.org/10.2480/AGRMET.42.309, 1987.

Sandoval, D.: dsval/rsplash: Simple process-led algorithms for simulating habitats (SPLASH v.2.0): calibration-free calculations of water and energy fluxes (GMD), Zenodo [code and data set], https://doi.org/10.5281/zenodo.10047627, 2023.

Sandoval, D., Prentice, I. C., and Nóbrega, R. L. B.: Simple process-led algorithms for simulating habitats (SPLASH v.2.0): robust calculations of water and energy fluxes, Geosci. Model Dev., 17, 4229–4309, https://doi.org/10.5194/gmd-17-4229-2024, 2024.

Savenije, H. H. G.: The importance of interception and why we should delete the term evapotranspiration from our vocabulary, Hydrological Processes, 18, 1507–1511, https://doi.org/10.1002/hyp.5563, 2004.

Scanlon, T. M. and Kustas, W. P.: Partitioning carbon dioxide and water vapor fluxes using correlation analysis, Agricultural and Forest Meteorology, 150, 89–99, https://doi.org/10.1016/J.AGRFORMET.2009.09.005, 2010.

Scanlon, T. M. and Kustas, W. P.: Partitioning Evapotranspiration Using an Eddy Covariance-Based Technique: Improved Assessment of Soil Moisture and Land–Atmosphere Exchange Dynamics, Vadose Zone Journal, 11, https://doi.org/10.2136/vzj2012.0025, 2012.

Scanlon, T. M. and Sahu, P.: On the correlation structure of water vapor and carbon dioxide in the atmospheric surface layer: A basis for flux partitioning, Water Resources Research, 44, 10418, https://doi.org/10.1029/2008WR006932, 2008.

Schenk, H. J. and Jackson, R. B.: The Global Biogeography of Roots, Ecological Monographs, 72, 311–328, https://doi.org/10.1890/0012-9615(2002)072[0311:TGBOR]2.0.CO;2, 2002.

Schlesinger, W. H. and Jasechko, S.: Transpiration in the global water cycle, Agricultural and Forest Meteorology, 189–190, 115–117, https://doi.org/10.1016/j.agrformet.2014.01.011, 2014.

Schymanski, S. J. and Or, D.: Wind increases leaf water use efficiency, Plant, Cell & Environment, 39, 1448–1459, https://doi.org/10.1111/pce.12700, 2016.

Scott, R. L. and Biederman, J. A.: Partitioning evapotranspiration using long-term carbon dioxide and water vapor fluxes, Geophysical Research Letters, 44, 6833–6840, https://doi.org/10.1002/2017GL074324, 2017.

Shan, N., Ju, W., Migliavacca, M., Martini, D., Guanter, L., Chen, J., Goulas, Y., and Zhang, Y.: Modeling canopy conductance and transpiration from solar-induced chlorophyll fluorescence, Agricultural and Forest Meteorology, 268, 189–201, https://doi.org/10.1016/J.AGRFORMET.2019.01.031, 2019.

Sivapalan, M., Yaeger, M. A., Harman, C. J., Xu, X., and Troch, P. A.: Functional model of water balance variability at the catchment scale: 1. Evidence of hydrologic similar-

ity and space-time symmetry, Water Resources Research, 47, https://doi.org/10.1029/2010WR009568, 2011.

Skaggs, T. H., Anderson, R. G., Alfieri, J. G., Scanlon, T. M., and Kustas, W. P.: Fluxpart: Open source software for partitioning carbon dioxide and water vapor fluxes, Agricultural and Forest Meteorology, 253–254, 218–224, https://doi.org/10.1016/J.AGRFORMET.2018.02.019, 2018.

Stocker, B. D., Wang, H., Smith, N. G., Harrison, S. P., Keenan, T. F., Sandoval, D., Davis, T., and Prentice, I. C.: P-model v1.0: an optimality-based light use efficiency model for simulating ecosystem gross primary production, Geosci. Model Dev., 13, 1545–1581, https://doi.org/10.5194/gmd-13-1545-2020, 2020.

Stoy, P. C., El-Madany, T. S., Fisher, J. B., Gentine, P., Gerken, T., Good, S. P., Klosterhalfen, A., Liu, S., Miralles, D. G., Perez-Priego, O., Rigden, A. J., Skaggs, T. H., Wohlfahrt, G., Anderson, R. G., Coenders-Gerrits, A. M. J., Jung, M., Maes, W. H., Mammarella, I., Mauder, M., Migliavacca, M., Nelson, J. A., Poyatos, R., Reichstein, M., Scott, R. L., and Wolf, S.: Reviews and syntheses: Turning the challenges of partitioning ecosystem evaporation and transpiration into opportunities, Biogeosciences, 16, 3747–3775, https://doi.org/10.5194/bg-16-3747-2019, 2019.

Swanson, R. H. and Whitfield, D. W. A.: A Numerical Analysis of Heat Pulse Velocity Theory and Practice, Journal of Experimental Botany, 32, 221–239, https://doi.org/10.1093/JXB/32.1.221, 1981.

Tan, S., Wang, H., Prentice, I. C., and Yang, K.: Land-surface evapotranspiration derived from a first-principles primary production model, Environmental Research Letters, 16, 104047, https://doi.org/10.1088/1748-9326/ac29eb, 2021.

Tang, Y. and Wang, D.: Evaluating the role of watershed properties in long-term water balance through a Budyko equation based on two-stage partitioning of precipitation, Water Resources Research, 53, 4142–4157, https://doi.org/10.1002/2016WR019920, 2017.

Thornton, M. M., Shrestha, R., Wei, Y., Thornton, P. E., Kao, S.-C., and Wilson, B. E.: Daymet: Daily Surface Weather Data on a 1-km Grid for North America, Version 4 R1, ORNL Distributed Active Archive Center [data set], https://doi.org/10.3334/ORNLDAAC/2129, 2022.

USDA SCS: National engineering handbook, Section 4, Hydrology, U.S. Dept. of Agriculture, Soil Conservation Service, Washington, D.C., https://ia601205.us.archive.org/27/items/CAT71334647003/CAT71334647003.pdf (last access: 7 September 2022), 1985.

Wallace, A., Romney, E. M., and Cha, J. W.: Depth Distribution of Roots of Some Perennial Plants in the Nevada Test Site Area of the Northern Mojave Desert, Great Basin Naturalist Memoirs, 201–207, https://www.jstor.org/stable/23376679 (last access: 12 October 2022), 1980.

Wang, D. and Tang, Y.: A one-parameter Budyko model for water balance captures emergent behavior in darwinian hydrologic models, Geophysical Research Letters, 41, 4569–4577, https://doi.org/10.1002/2014GL060509, 2014.

Wang, D., Zhao, J., Tang, Y., and Sivapalan, M.: A thermodynamic interpretation of Budyko and L'Vovich formulations of annual water balance: Proportionality Hypothesis and maximum entropy production, Water Resources Research, 51, 3007–3016, https://doi.org/10.1002/2014WR016857, 2015.

Wang, H., Prentice, I. C., Keenan, T. F., Davis, T. W., Wright, I. J., Cornwell, W. K., Evans, B. J., and Peng, C.: Towards a universal model for carbon dioxide uptake by plants, Nature Plants, 3, 734–741, https://doi.org/10.1038/s41477-017-0006-8, 2017.

Wang, L., Good, S. P., and Caylor, K. K.: Global synthesis of vegetation control on evapotranspiration partitioning, Geophysical Research Letters, 41, 6753–6757, https://doi.org/10.1002/2014GL061439, 2014.

Wang, Y., Zhang, Y., Yu, X., Jia, G., Liu, Z., Sun, L., Zheng, P., and Zhu, X.: Grassland soil moisture fluctuation and its relationship with evapotranspiration, Ecological Indicators, 131, https://doi.org/10.1016/j.ecolind.2021.108196, 2021.

Wei, Z., Yoshimura, K., Wang, L., Miralles, D. G., Jasechko, S., and Lee, X.: Revisiting the contribution of transpiration to global terrestrial evapotranspiration, Geophysical Research Letters, 44, 2792–2801, https://doi.org/10.1002/2016GL072235, 2017.

Williams, D. G., Cable, W., Hultine, K., Hoedjes, J. C. B., Yepez, E. A., Simonneaux, V., Er-Raki, S., Boulet, G., De Bruin, H. A. R., Chehbouni, A., Hartogensis, O. K., and Timouk, F.: Evapotranspiration components determined by stable isotope, sap flow and eddy covariance techniques, Agricultural and Forest Meteorology, 125, 241–258, https://doi.org/10.1016/J.AGRFORMET.2004.04.008, 2004.

Williamson, M. S., Thackeray, C. W., Cox, P. M., Hall, A., Huntingford, C., and Nijsse, F. J. M. M.: Emergent constraints on climate sensitivities, Reviews of Modern Physics, 93, https://doi.org/10.1103/RevModPhys.93.025004, 2021.

Xie, J., Liu, X., Wang, K., Yang, T., Liang, K., and Liu, C.: Evaluation of typical methods for baseflow separation in the contiguous United States, Journal of Hydrology, 583, 124628, https://doi.org/10.1016/J.JHYDROL.2020.124628, 2020.

Yu, L., Zhou, S., Zhao, X., Gao, X., Jiang, K., Zhang, B., Cheng, L., Song, X., and Siddique, K. H. M.: Evapotranspiration Partitioning Based on Leaf and Ecosystem Water Use Efficiency, Water Resources Research, 58, https://doi.org/10.1029/2021WR030629, 2022.

Zeng, X.: Global Vegetation Root Distribution for Land Modeling, Journal of Hydrometeorology, 2, 525–530, https://doi.org/10.1175/1525-7541(2001)002<0525:GVRDFL>2.0.CO;2, 2001.

Zhang, J., Duan, L., Liu, T., Chen, Z., Wang, Y., Li, M., and Zhou, Y.: Experimental analysis of soil moisture response to rainfall in a typical grassland hillslope under different vegetation treatments, Environmental Research, 213, https://doi.org/10.1016/j.envres.2022.113608, 2022.

Zhang, K., Kimball, J. S., Nemani, R. R., and Running, S. W.: A continuous satellite-derived global record of land surface evapotranspiration from 1983 to 2006, Water Resources Research, 46, 9522, https://doi.org/10.1029/2009WR008800, 2010.

Zhang, Y., Shen, Y., Sun, H., and Gates, J. B.: Evapotranspiration and its partitioning in an irrigated winter wheat field: A combined isotopic and micrometeorologic approach, Journal of Hydrology, 408, 203–211, https://doi.org/10.1016/J.JHYDROL.2011.07.036, 2011.

Zhou, B., Cai, W., Zhu, Z., Wang, H., Harrison, S. P., and Prentice, I. C.: A General Model for the Seasonal to Decadal Dynamics of Leaf Area, Global Change Biology, 31, https://doi.org/10.1111/gcb.70125, 2025.

Zhou, S., Yu, B., Zhang, Y., Huang, Y., and Wang, G.: Partitioning evapotranspiration based on the concept of underlying water use efficiency, Water Resources Research, 52, 1160–1175, https://doi.org/10.1002/2015WR017766, 2016.